JOURNAL OF THERMOPHYSICS AND HEAT TRANSFER
Vol. 15, No. 1, January–March 2001

# Chemical-Kinetic Parameters of Hyperbolic Earth Entry

Chul Park*
*Eloret Corporation, Moffett Field, California 94085*
and
Richard L. Jaffe† and Harry Partridge‡
*NASA Ames Research Center, Moffett Field, California 94035*

**Chemical-kinetic parameters governing the flow in the shock layer over a heat shield of a blunt body entering Earth's atmosphere from a hyperbolic orbit are derived. By the use of the assumption that the heat shield is made of carbon phenolic and by allowing for an arbitrary rate of pyrolysis-gas injection, chemical reactions occurring in the shock layer are postulated, and the collision integrals governing the transport properties, the rate coefficients of the reactions, and the parameters needed for the bifurcation model and for the finite-rate kinetic wall boundary conditions are determined using the best available techniques. Sample flowfield calculations are performed using this set of parameters to show that the heating and surface removal rates are substantially smaller than calculated using the existing set of such parameters and traditional assumptions of gas–surface equilibrium and quasi-steady-state ablation.**

## Nomenclature

$A_i$ = coefficient in equilibrium constant; Eq. (12)
$C$ = reaction rate coefficient; Eq. (9)
$D_{ij}$ = binary diffusion coefficient between species $i$ and $j$, $cm^2/s$ or $m^2/s$
$\bar{D}$ = reference diffusion coefficient; Eq. (5)
$d$ = collision diameter, cm
$F_i$ = parameter in bifurcation model; Eq. (5)
$I_i$ = number flux of species $i$, $cm^{-2} \cdot s^{-1}$ or $m^{-2} \cdot s^{-1}$
$J_i$ = mass flux of species $i$, $g/(cm^2 \cdot s)$ or $kg/(m^2 \cdot s)$
$K_e$ = equilibrium constant
$k$ = Boltzmann constant, $1.3806 \times 10^{-16}$ erg/K
$k_f$ = forward rate coefficient, $cm^3/(mol\text{-}s)$
$k_w$ = surface reaction velocity, cm/s or m/s; Eq. (16)
$M$ = third body
$M_i$ = molar mass of species $i$, g/mol or kg/mol
$\bar{M}$ = average molar mass, g/mol or kg/mol
$m$ = mass of one particle, g or kg
$\dot{m}$ = mass flux (ablation rate), $g/(cm^2 s)$ or $kg/(m^2 \cdot s)$
$\dot{m}_p$ = pyrolysis gas injection rate, $g/(cm^2 \cdot s)$ or $kg/(m^2 \cdot s)$
$\dot{m}_w$ = rate of surface removal, $g/(cm^2 \cdot s)$ or $kg/(m^2 \cdot s)$
$\dot{m}_{w,i}$ = rate of surface reaction $i$, $g/(cm^2 \cdot s)$ or $kg/(m^2 \cdot s)$
$n$ = reaction rate exponent; Eq. (9)
$n_t$ = total number density, $cm^{-3}$ or $m^{-3}$
$Pr$ = Prandtl number
$p$ = pressure, dyne/$cm^2$ or Pa
$q$ = convective heating rate, $W/m^2$
$R$ = nose radius, m
$\bar{S}c$ = reference Schmidt number
$T$ = translational–rotational temperature, K
$T_a$ = controlling temperature, K
$T_e$ = electron temperature, K
$T_r$ = reaction activation temperature, K; Eq. (9)
$T_v$ = vibrational-electron-electronic temperature, K
$v$ = velocity in $y$ direction, cm/s or m/s
$X_i$ = molar fraction of species $i$
$y$ = distance from wall, m or mm
$Z_i$ = equivalent species variable; Eq. (7)
$z_i$ = mass fraction of species $i$
$\alpha_i$ = surface reaction probability; Eqs. (17a–17i)
$\gamma_i$ = concentration of species $i$, mol/g or mol/kg
$\epsilon$ = attractive potential well depth, erg
$\mu$ = viscosity, $m^2/s$
$\mu_1, \mu_2$ = parameter in bifurcation model; Eq. (8)
$\rho$ = gas density, $g/cm^3$ or $kg/m^3$
$\sigma$ = standard deviation
$\Omega^{(l,s)}$ = collision integral, $cm^2$

*Subscripts*

$E$ = equilibrium
$f$ = forward reaction
$i$ = species $i$
$p$ = pyrolysis gas
$r$ = reverse reaction
$w$ = wall surface
$\infty$ = freestream

## Introduction

IN the future, spacecraft are expected to bring samples of planetary, asteroidal, or cometary materials and enter Earth's atmosphere at a hyperbolic flight speed.[1–4] A crewed flight to and from Mars is also a possibility. For such hyperbolic entries, the heating rates are such that ablation of the heat shield material occurs to a substantial extent. It is desirable that the ablative heat shields for those hyperbolic Earth entry vehicles are designed with a high precision, so that the weight of the entry vehicle is kept to a minimum.

In Ref. 5, the accuracy of characterizing the heating environment of an ablating heat shield is analyzed for the three missions for which the heating and ablating environment was monitored, namely, the Apollo 4 and 6, the Pioneer-Venus Probes, and the Galileo Probe. It was shown that, for all three missions, the state-of-the-art method erred by a substantial margin. This is in contrast to the case of nonablating heat shield, for which calculation closely reproduced the flight data (e.g., see Ref. 6.)

Over an ablating heat shield, the flowfield contains the gas species originating in the heat shield material. One reason for the difficulty in predicting the heating-ablating environment for such a flowfield

Presented as Paper 2000-0210 at the AIAA 38th Aerospace Sciences Meeting, Reno, NV, 10–13 January 2000; received 4 April 2000; revision received 5 July 2000; accepted for publication 28 July 2000. 

*Senior Research Scientist, Space Technology Division; Mail Stop 229-1, NASA Ames Research Center, Moffett Field, CA 94035. AIAA Fellow.
†Research Scientist, Computational Chemistry Branch. Associate Fellow AIAA.
‡Research Scientist, Computational Chemistry Branch.

is that the chemical reaction rates, both gas phase and gas to surface, the transport properties, and the phenomena occurring at the wall are not well known.

It is the purpose of the present work to compile a best estimate of those chemical parameters presently possible. The paper includes 1) compilation of the collision integrals among the species that control transport properties, 2) compilation of gas-phase reaction rates, and 3) characterization of the gas–surface nonequilibrium phenomenon. Additionally, solutions of the stagnation-region flowfield obtained with the present set of parameters will be shown and compared with a solution obtained previously with a traditional method.

## Chemical Species

### Description of Ablation Phenomenon

The phenomenon of ablation of a carbonaceous heat shield is well known. A few seconds after the commencement of the heating pulse during an entry flight, the surface of the heat shield becomes char. The surface of the char then vaporizes through sublimation, oxidation, and possibly by combining with atomic nitrogen to form CN (Ref. 5). The vaporization of the char surface represents surface removal. Thus, the ablation product injected into the flow consists of two components: the pyrolysis gas and the vapor originating from the char.

One major assumption made in the past analyses of the gas-phase properties of the shock layer over an ablating heat shield was the assumption of quasi-steady-state ablation, which states that the ratio of the mass fluxes between the pyrolysis gas and the gaseous carbon from the surface is the mass ratio between the two components in the virgin material (e.g., see Ref. 7). After the flight of the Apollo vehicle, it was found that surface removal was small, but the depth of the char was large.[8] This implies that the steady-state ablation condition was not reached throughout the most of the flight, and the flux of the pyrolysis gas is relatively larger than calculated by the assumption of quasi-steady-state ablation.

This large flux of pyrolysis gas affects the flowfield in two ways. First, the total mass flux of the ablation product is larger, which leads to a larger convective and radiative blockage. Second, the chemical composition of the boundary layer is different: Notably, a substantial concentration of hydrogen is released from the pyrolysis gas. Because hydrogen species have kinetic properties very different from other species, a substantial change in flowfield behavior will occur by the large pyrolysis-gas injection. Thus, there is a need to calculate the ablation phenomenon under an arbitrarily high rate of pyrolysis-gas injection.

### Pyrolysis-Gas Composition

For a more accurate characterization of the ablation phenomenon, it is necessary to characterize the behavior of the gas species produced by the pyrolysis phenomenon. An attempt to do so was made in Ref. 9, wherein the motion of the pyrolysis gas inside the heat shield material was calculated. The calculation showed that the speed of the pyrolysis gas inside the material is only of the order of 10 m/s. In this environment, it is likely that the pyrolysis gas is in equilibrium at the local temperature of the char. Therefore, when the pyrolysis gas leaves the material surface, its composition is likely to be that of an equilibrium vapor at the wall pressure and temperature.

The wall temperature in a typical Apollo-like environment is about 3000 K. At the edge of the boundary layer, it reaches up to about 12,000 K. The equilibrium compositions of the pyrolysis gas are calculated here for this temperature range for a typical carbon-phenolic and the Avcoat 5026-39 HC/G used for the Apollo vehicles.[8] The ratio of the elemental masses in the pyrolysis gas is taken for the carbon phenolic from Ref. 10 to be H:C:O = 0.1285:0.5315:0.3400. For Avcoat, the elemental ratio is H:C:N:O = 0.0930:0.5470:0.0190:0.0340 (Ref. 11).

In Figs. 1a and 1b, the equilibrium compositions of the pyrolysis gas for these two materials are shown. In the calculation of the equilibrium compositions for the typical carbon phenolic, in addition to the species seen in Figs. 1, $O_2$, OH, $HO_2$, $H_2O$, $CH_2$, $CH_3$, $H_2O_2$, $C_4$, $CH_4$, $C_5$, and $C_5H$ were also considered. However, their

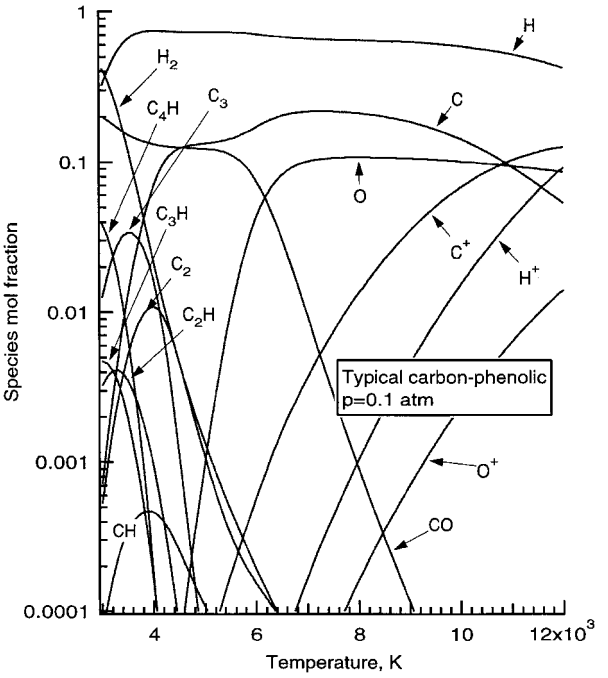


**a) Typical carbon phenolic, H:C:O = 0.1285:0.5315:0.3400**

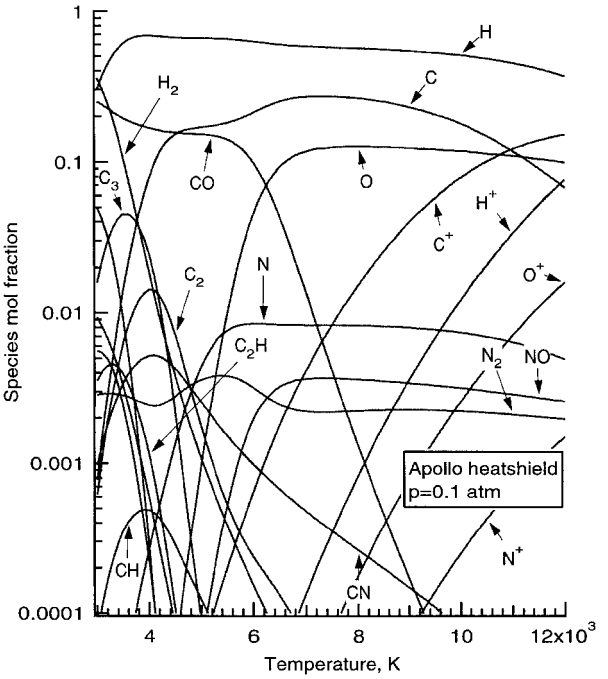


**b) Apollo heat shield material (Avcoat 5026-39 HC/G), C:H:N:O = 0.5470:0.0930:0.0190:03410**

**Fig. 1 Equilibrium composition of pyrolysis gas. (The species not shown have a concentration below the shown lower limit.)**

concentrations are too small to appear in Figs. 1. For Avcoat, NH, HCN, and CNO were also included, but their concentrations are also too small to appear in Figs. 1. $CO_2$ was not considered because its formation at the wall surface is unlikely (see "Surface Reaction Rates" subsection), and, in the gas phase, the temperature is too high to form $CO_2$ from CO and O.

Figures 1a and 1b show that the major species in the boundary layer are C, H, O, $H_2$, $C_2$, CO, $C_2H$, $C_3$, $C^+$, and $H^+$ for both materials. Therefore, at least these species must be accounted for in the calculation of the flowfield. For Avcoat, CN is also a major species. Even for the carbon phenolic, which does not contain N, CN is likely to be formed by the interaction of carbonaceous species and nitrogen species. Therefore, CN must be included in the species set

for both materials. $C_3$ and $C_2H$ must be included for the additional reason that they have strong optical absorptive properties.[12,13]

This species set now must be combined with that of ionized air for a complete description of the shock layer flow. Ionized air contains $O_2^+$. However, $O_2^+$ can be ignored because it is produced only to a small concentration and does not play any significant role in chemical reaction scheme or in radiation. $N_2^+$ radiates strongly and, therefore, must be considered. Thus, there are 20 chemical species that need to be considered in the flowfield calculation: C, O, N, H, CO, $C_2$, $N_2$, CN, NO, $O_2$, $H_2$, $C_3$, $C_2H$, $C^+$, $H^+$, $O^+$, $N^+$, $NO^+$, $N_2^+$, and $e^-$.

## Transport Properties

The 20 chemical species in the flowfield produce 190 collision pairs. For this many collision pairs, one must be content with a first-order approximation to the transport properties. The first-order transport properties are determined by the collision integrals $\Omega^{(1,1)}$ and $\Omega^{(2,2)}$ (e.g., see Ref. 14). Quantum-mechanical determination of the collision integrals have been made only for a limited number of these collision pairs. In the present work, all available quantum-mechanical data on those collision pairs were collected. For those collision pairs for which quantum-mechanical calculations have not yet been made, collision integrals have been estimated with the best available method. The collision integral values so determined are listed in Tables 1 and 2.

### Recent Quantum-Mechanical Calculations

The collision pairs for which quantum-mechanical calculations have been performed in recent years are N–N (Ref. 15), N–O (Ref. 15), O–O (Ref. 15), N–H (Ref. 16), $N–N^+$ (Ref. 17), $N–O^+$ (Ref. 18), $O–N^+$ (Ref. 18), $O–O^+$ (Ref. 17), $N_2–H$ (Ref. 19), $H–H_2$ (Ref. 20), C–C (Ref. 21), and C–N (Ref. 21). These values are given in Tables 1 and 2 and are identified as being determined by method a.

### Earlier Quantum-Mechanical Calculations for Electron-Neutral Atom Collisions

For e–H (Ref. 22), e–O (Ref. 23), e–N (Ref. 24), and e–C (Ref. 25) encounters, quantum-mechanical calculations have been made of the differential cross sections. The accuracy of these calculations have been verified by comparing with experiments.[22–25] The collision integrals are calculated using these differential cross section values in the present work. This method of determining collision integrals is referred to as method b.

### Ion-Neutral Collisions

For the ion-neutral collisions for which no quantum-mechanical solutions exist, Ref. 14 provides an approximate method of estimation by which all such collisions produce the same values of collision integrals. This method is used for collisions between $C^+$ and $H^+$ with neutrals. This method is identified as method c.

**Table 1 Common logarithm of the collision integrals $\pi\Omega^{(1,1)}$ excluding collision pairs listed in Ref. 14**

| Collision pair | | $T$ | | | | | | Collision pair | | $T$ | | | | | |
|---|---|---|---|---|---|---|---|---|---|---|---|---|---|---|---|
| | | 2,000 | 4,000 | 8,000 | 16,000 | 32,000 | Method | | | 2,000 | 4,000 | 8,000 | 16,000 | 32,000 | Method |
| C | C | −14.65 | −14.74 | −14.84 | −15.00 | −15.18 | a | $H_2$ | C | −14.80 | −14.92 | −15.04 | −15.17 | −15.29 | d |
| O | C | −14.75 | −14.87 | −14.99 | −15.12 | −15.24 | d | $H_2$ | O | −14.81 | −14.93 | −15.05 | −15.17 | −15.29 | d |
| O | O | −14.82 | −14.90 | −14.99 | −15.09 | −15.18 | a | $H_2$ | N | −14.78 | −14.91 | −15.03 | −15.15 | −15.27 | d |
| N | C | −14.75 | −14.82 | −14.90 | −15.02 | −15.19 | a | $H_2$ | H | −15.05 | −15.20 | −15.38 | −15.59 | −15.79 | a |
| N | O | −14.78 | −14.85 | −14.94 | −15.04 | −15.16 | a | $H_2$ | CO | −14.72 | −14.84 | −14.96 | −15.09 | −15.21 | d |
| N | N | −14.79 | −14.86 | −14.95 | −15.05 | −15.17 | a | $H_2$ | $C_2$ | −14.70 | −14.82 | −14.94 | −15.06 | −15.18 | d |
| H | C | −14.83 | −14.95 | −15.08 | −15.20 | −15.32 | d | $H_2$ | $N_2$ | −14.72 | −14.84 | −14.96 | −15.08 | −15.20 | d |
| H | O | −14.84 | −14.96 | −15.08 | −15.21 | −15.33 | d | $H_2$ | CN | −14.71 | −14.83 | −14.95 | −15.07 | −15.19 | d |
| H | N | −14.76 | −14.85 | −14.97 | −15.15 | −15.38 | a | $H_2$ | NO | −14.73 | −14.86 | −14.98 | −15.10 | −15.22 | d |
| H | H | −14.88 | −15.00 | −15.14 | −15.26 | −15.43 | e | $H_2$ | $O_2$ | −14.75 | −14.87 | −14.99 | −15.11 | −15.23 | d |
| CO | C | −14.67 | −14.79 | −14.92 | −15.04 | −15.16 | d | $H_2$ | $H_2$ | −14.87 | −14.97 | −15.16 | −15.23 | −15.42 | e |
| CO | O | −14.67 | −14.79 | −14.92 | −15.04 | −15.16 | d | $C_3$ | C | −14.67 | −14.79 | −14.91 | −15.04 | −15.16 | d |
| CO | N | −14.65 | −14.78 | −14.90 | −15.02 | −15.14 | d | $C_3$ | O | −14.67 | −14.79 | −14.92 | −15.04 | −15.16 | d |
| CO | H | −14.75 | −14.88 | −15.00 | −15.12 | −15.24 | d | $C_3$ | N | −14.65 | −14.77 | −14.90 | −15.02 | −15.14 | d |
| CO | CO | −14.60 | −14.72 | −14.84 | −14.96 | −15.09 | d | $C_3$ | H | −14.76 | −14.88 | −15.00 | −15.12 | −15.24 | d |
| $C_2$ | C | −14.65 | −14.77 | −14.89 | −15.02 | −15.14 | d | $C_3$ | CO | −14.59 | −14.71 | −14.84 | −14.96 | −15.08 | d |
| $C_2$ | O | −14.65 | −14.77 | −14.89 | −15.01 | −15.14 | d | $C_3$ | $C_2$ | −14.57 | −14.69 | −14.81 | −14.94 | −15.06 | d |
| $C_2$ | N | −14.63 | −14.75 | −14.88 | −15.00 | −15.12 | d | $C_3$ | $N_2$ | −14.59 | −14.71 | −14.83 | −14.95 | −15.08 | d |
| $C_2$ | H | −14.73 | −14.85 | −14.97 | −15.09 | −15.22 | d | $C_3$ | CN | −14.58 | −14.70 | −14.82 | −14.95 | −15.07 | d |
| $C_2$ | CO | −14.58 | −14.70 | −14.82 | −14.94 | −15.07 | d | $C_3$ | NO | −14.60 | −14.73 | −14.85 | −14.97 | −15.09 | d |
| $C_2$ | $C_2$ | −14.56 | −14.68 | −14.80 | −14.92 | −15.05 | d | $C_3$ | $O_2$ | −14.61 | −14.74 | −14.86 | −14.98 | −15.10 | d |
| $N_2$ | C | −14.67 | −14.79 | −14.91 | −15.03 | −15.16 | d | $C_3$ | $H_2$ | −14.72 | −14.84 | −14.97 | −15.09 | −15.21 | d |
| $N_2$ | H | −14.82 | −14.95 | −15.12 | −15.30 | −15.47 | a | $C_3$ | $C_3$ | −14.57 | −14.71 | −14.83 | −14.96 | −15.08 | d |
| $N_2$ | CO | −14.59 | −14.72 | −14.84 | −14.96 | −15.08 | d | $C_2H$ | C | −14.67 | −14.79 | −14.91 | −15.04 | −15.16 | d |
| $N_2$ | $C_2$ | −14.57 | −14.70 | −14.82 | −14.94 | −15.06 | d | $C_2H$ | O | −14.67 | −14.79 | −14.92 | −15.04 | −15.16 | d |
| CN | C | −14.66 | −14.78 | −14.90 | −15.02 | −15.15 | d | $C_2H$ | N | −14.65 | −14.77 | −14.90 | −15.02 | −15.14 | d |
| CN | O | −14.66 | −14.78 | −14.90 | −15.02 | −15.15 | d | $C_2H$ | H | −14.76 | −14.88 | −15.00 | −15.12 | −15.24 | d |
| CN | N | −14.64 | −14.76 | −14.88 | −15.01 | −15.13 | d | $C_2H$ | CO | −14.59 | −14.71 | −14.84 | −14.96 | −15.08 | d |
| CN | H | −14.74 | −14.86 | −14.98 | −15.10 | −15.23 | d | $C_2H$ | $C_2$ | −14.57 | −14.69 | −14.81 | −14.94 | −15.06 | d |
| CN | CO | −14.59 | −14.71 | −14.83 | −14.95 | −15.07 | d | $C_2H$ | $N_2$ | −14.59 | −14.71 | −14.83 | −14.95 | −15.08 | d |
| CN | $C_2$ | −14.57 | −14.69 | −14.81 | −14.93 | −15.05 | d | $C_2H$ | CN | −14.58 | −14.70 | −14.82 | −14.95 | −15.07 | d |
| CN | $N_2$ | −14.58 | −14.70 | −14.83 | −14.95 | −15.07 | d | $C_2H$ | NO | −14.60 | −14.73 | −14.85 | −14.97 | −15.09 | d |
| CN | CN | −14.57 | −14.70 | −14.82 | −14.94 | −15.06 | d | $C_2H$ | $O_2$ | −14.61 | −14.74 | −14.86 | −14.98 | −15.10 | d |
| NO | C | −14.68 | −14.81 | −14.93 | −15.05 | −15.17 | d | $C_2H$ | $H_2$ | −14.72 | −14.84 | −14.97 | −15.09 | −15.21 | d |
| NO | H | −14.77 | −14.89 | −15.01 | −15.13 | −15.25 | d | $C_2H$ | $C_3$ | −14.57 | −14.71 | −14.83 | −14.96 | −15.08 | d |
| NO | CO | −14.61 | −14.73 | −14.85 | −14.98 | −15.10 | d | $C_2H$ | $C_2H$ | −14.57 | −14.71 | −14.83 | −14.96 | −15.08 | d |
| NO | $C_2$ | −14.59 | −14.71 | −14.83 | −14.95 | −15.08 | d | $C^+$ | C | −14.34 | −14.46 | −14.58 | −14.70 | −14.83 | c |
| NO | CN | −14.60 | −14.72 | −14.84 | −14.96 | −15.08 | d | $C^+$ | O | −14.34 | −14.46 | −14.58 | −14.70 | −14.83 | c |
| $O_2$ | C | −14.69 | −14.82 | −14.94 | −15.06 | −15.18 | d | $C^+$ | N | −14.34 | −14.46 | −14.58 | −14.70 | −14.83 | c |
| $O_2$ | H | −14.78 | −14.90 | −15.02 | −15.14 | −15.27 | d | $C^+$ | H | −14.34 | −14.46 | −14.58 | −14.70 | −14.83 | c |
| $O_2$ | CO | −14.62 | −14.74 | −14.86 | −14.99 | −15.11 | d | $C^+$ | CO | −14.34 | −14.46 | −14.58 | −14.70 | −14.83 | c |
| $O_2$ | $C_2$ | −14.60 | −14.72 | −14.84 | −14.96 | −15.09 | d | $C^+$ | $C_2$ | −14.50 | −14.62 | −14.74 | −14.86 | −14.99 | d |
| $O_2$ | CN | −14.61 | −14.73 | −14.85 | −14.97 | −15.09 | d | $C^+$ | $N_2$ | −14.34 | −14.46 | −14.58 | −14.70 | −14.83 | c |

(Continued)

**Table 1 Common logarithm of the collision integrals $\pi\Omega^{(1,1)}$ excluding collision pairs listed in Ref. 14 (continued)**

| Collision pair | | $T$ 2,000 | 4,000 | 8,000 | 16,000 | 32,000 | Method | Collision pair | | $T$ 2,000 | 4,000 | 8,000 | 16,000 | 32,000 | Method |
|---|---|---|---|---|---|---|---|---|---|---|---|---|---|---|---|
| $C^+$ | CN | −14.34 | −14.46 | −14.58 | −14.70 | −14.83 | c | $N^+$ | $C_2$ | −14.34 | −14.46 | −14.58 | −14.70 | −14.83 | c |
| $C^+$ | NO | −14.34 | −14.46 | −14.58 | −14.70 | −14.83 | c | $N^+$ | CN | −14.34 | −14.46 | −14.58 | −14.70 | −14.83 | c |
| $C^+$ | $O_2$ | −14.34 | −14.46 | −14.58 | −14.70 | −14.83 | c | $N^+$ | $H_2$ | −14.34 | −14.46 | −14.58 | −14.70 | −14.83 | c |
| $C^+$ | $H_2$ | −14.34 | −14.46 | −14.58 | −14.70 | −14.83 | c | $N^+$ | $C_3$ | −14.34 | −14.46 | −14.58 | −14.70 | −14.83 | c |
| $C^+$ | $C_3$ | −14.34 | −14.46 | −14.58 | −14.70 | −14.83 | c | $N^+$ | $C_2H$ | −14.34 | −14.46 | −14.58 | −14.70 | −14.83 | c |
| $C^+$ | $C_2H$ | −14.34 | −14.46 | −14.58 | −14.70 | −14.83 | c | $N^+$ | $C^+$ | −11.48 | −12.08 | −12.68 | −13.28 | −13.76 | f |
| $C^+$ | $C^+$ | −11.48 | −12.08 | −12.68 | −13.28 | −13.76 | f | $N^+$ | $H^+$ | −11.48 | −12.08 | −12.68 | −13.28 | −13.76 | f |
| $H^+$ | C | −14.34 | −14.46 | −14.58 | −14.70 | −14.83 | c | $NO^+$ | C | −14.34 | −14.46 | −14.58 | −14.70 | −14.83 | c |
| $H^+$ | O | −14.34 | −14.46 | −14.58 | −14.70 | −14.83 | c | $NO^+$ | H | −14.34 | −14.46 | −14.58 | −14.70 | −14.83 | c |
| $H^+$ | N | −14.34 | −14.46 | −14.58 | −14.70 | −14.83 | c | $NO^+$ | CO | −14.34 | −14.46 | −14.58 | −14.70 | −14.83 | c |
| $H^+$ | H | −13.94 | −13.97 | −14.03 | −14.61 | −15.11 | e | $NO^+$ | $C_2$ | −14.34 | −14.46 | −14.58 | −14.70 | −14.83 | c |
| $H^+$ | CO | −14.34 | −14.46 | −14.58 | −14.70 | −14.83 | c | $NO^+$ | CN | −14.34 | −14.46 | −14.58 | −14.70 | −14.83 | c |
| $H^+$ | $C_2$ | −14.59 | −14.71 | −14.84 | −14.96 | −15.08 | d | $NO^+$ | $H_2$ | −14.34 | −14.46 | −14.58 | −14.70 | −14.83 | c |
| $H^+$ | $N_2$ | −14.34 | −14.46 | −14.58 | −14.70 | −14.83 | c | $NO^+$ | $C_3$ | −14.34 | −14.46 | −14.58 | −14.70 | −14.83 | c |
| $H^+$ | CN | −14.34 | −14.46 | −14.58 | −14.70 | −14.83 | c | $NO^+$ | $C_2H$ | −14.34 | −14.46 | −14.58 | −14.70 | −14.83 | c |
| $H^+$ | NO | −14.34 | −14.46 | −14.58 | −14.70 | −14.83 | c | $NO^+$ | $C^+$ | −11.48 | −12.08 | −12.68 | −13.28 | −13.76 | f |
| $H^+$ | $O_2$ | −14.34 | −14.46 | −14.58 | −14.70 | −14.83 | c | $NO^+$ | $H^+$ | −11.48 | −12.08 | −12.68 | −13.28 | −13.76 | f |
| $H^+$ | $H_2$ | −14.34 | −14.46 | −14.58 | −14.70 | −14.83 | c | $N_2^+$ | C | −14.34 | −14.46 | −14.58 | −14.70 | −14.83 | c |
| $H^+$ | $C_3$ | −14.34 | −14.46 | −14.58 | −14.70 | −14.83 | c | $N_2^+$ | H | −14.34 | −14.46 | −14.58 | −14.70 | −14.83 | c |
| $H^+$ | $C_2H$ | −14.34 | −14.46 | −14.58 | −14.70 | −14.83 | c | $N_2^+$ | CO | −14.34 | −14.46 | −14.58 | −14.70 | −14.83 | c |
| $H^+$ | $C^+$ | −11.48 | −12.08 | −12.68 | −13.28 | −13.76 | f | $N_2^+$ | $C_2$ | −14.34 | −14.46 | −14.58 | −14.70 | −14.83 | c |
| $H^+$ | $H^+$ | −11.48 | −12.08 | −12.68 | −13.28 | −13.76 | f | $N_2^+$ | CN | −14.34 | −14.46 | −14.58 | −14.70 | −14.83 | c |
| $O^+$ | C | −14.34 | −14.46 | −14.58 | −14.70 | −14.83 | c | $N_2^+$ | $H_2$ | −14.34 | −14.46 | −14.58 | −14.70 | −14.83 | c |
| $O^+$ | O | −14.11 | −14.15 | −14.17 | −14.20 | −14.23 | a | $N_2^+$ | $C_3$ | −14.34 | −14.46 | −14.58 | −14.70 | −14.83 | c |
| $O^+$ | N | −14.54 | −14.64 | −14.76 | −14.92 | −15.10 | a | $N_2^+$ | $C_2H$ | −14.34 | −14.46 | −14.58 | −14.70 | −14.83 | c |
| $O^+$ | H | −14.34 | −14.46 | −14.58 | −14.70 | −14.83 | c | $N_2^+$ | $C^+$ | −11.48 | −12.08 | −12.68 | −13.28 | −13.76 | f |
| $O^+$ | CO | −14.34 | −14.46 | −14.58 | −14.70 | −14.83 | c | $N_2^+$ | $H^+$ | −11.48 | −12.08 | −12.68 | −13.28 | −13.76 | f |
| $O^+$ | $C_2$ | −14.34 | −14.46 | −14.58 | −14.70 | −14.83 | c | $e^-$ | C | −14.44 | −14.36 | −14.38 | −14.39 | −14.38 | b |
| $O^+$ | CN | −14.34 | −14.46 | −14.58 | −14.70 | −14.83 | c | $e^-$ | O | −15.65 | −15.43 | −15.20 | −15.04 | −14.97 | b |
| $O^+$ | $H_2$ | −14.34 | −14.46 | −14.58 | −14.70 | −14.83 | c | $e^-$ | N | −14.73 | −14.67 | −14.60 | −14.54 | −14.41 | b |
| $O^+$ | $C_3$ | −14.34 | −14.46 | −14.58 | −14.70 | −14.83 | c | $e^-$ | H | −14.67 | −14.74 | −14.84 | −14.90 | −14.93 | b |
| $O^+$ | $C_2H$ | −14.34 | −14.46 | −14.58 | −14.70 | −14.83 | c | $e^-$ | CO | −15.29 | −15.06 | −14.94 | −15.11 | −15.78 | g |
| $O^+$ | $C^+$ | −11.48 | −12.08 | −12.68 | −13.28 | −13.76 | f | $e^-$ | $C_2$ | −15.29 | −15.06 | −14.94 | −15.11 | −15.78 | g |
| $O^+$ | $H^+$ | −11.48 | −12.08 | −12.68 | −13.28 | −13.76 | f | $e^-$ | CN | −15.29 | −15.06 | −14.94 | −15.11 | −15.78 | g |
| $N^+$ | C | −14.34 | −14.46 | −14.58 | −14.70 | −14.83 | c | $e^-$ | $H_2$ | −14.87 | −14.81 | −14.78 | −14.78 | −14.86 | e |
| $N^+$ | O | −14.58 | −14.71 | −14.87 | −15.04 | −15.21 | a | $e^-$ | $C_3$ | −15.29 | −15.06 | −14.94 | −15.11 | −15.78 | g |
| $N^+$ | N | −14.01 | −14.04 | −14.07 | −14.11 | −14.14 | a | $e^-$ | $C_2H$ | −15.29 | −15.06 | −14.94 | −15.11 | −15.78 | g |
| $N^+$ | H | −14.34 | −14.46 | −14.58 | −14.70 | −14.83 | c | $e^-$ | $C^+$ | −11.48 | −12.08 | −12.68 | −13.28 | −13.76 | f |
| $N^+$ | CO | −14.34 | −14.46 | −14.58 | −14.70 | −14.83 | c | $e^-$ | $H^+$ | −11.48 | −12.08 | −12.68 | −13.28 | −13.76 | f |

**Table 2 Common logarithm of the collision integrals $\pi\Omega^{(2,2)}$ excluding collision pairs listed in Ref. 14**

| Collision pair | | $T$ 2,000 | 4,000 | 8,000 | 16,000 | 32,000 | Method | Collision pair | | $T$ 2,000 | 4,000 | 8,000 | 16,000 | 32,000 | Method |
|---|---|---|---|---|---|---|---|---|---|---|---|---|---|---|---|
| C | C | −14.61 | −14.70 | −14.79 | −14.92 | −15.11 | a | CN | C | −14.61 | −14.73 | −14.84 | −14.96 | −15.08 | d |
| O | C | −14.70 | −14.82 | −14.94 | −15.05 | −15.17 | d | CN | O | −14.61 | −14.73 | −14.85 | −14.97 | −15.08 | d |
| O | O | −14.76 | −14.83 | −14.91 | −15.01 | −15.09 | a | CN | N | −14.59 | −14.71 | −14.83 | −14.95 | −15.07 | d |
| N | C | −14.70 | −14.78 | −14.85 | −14.94 | −15.10 | a | CN | H | −14.69 | −14.80 | −14.92 | −15.04 | −15.16 | d |
| N | O | −14.72 | −14.79 | −14.87 | −14.96 | −15.08 | a | CN | CO | −14.54 | −14.66 | −14.77 | −14.89 | −15.01 | d |
| N | N | −14.74 | −14.81 | −14.89 | −14.98 | −15.09 | a | CN | $C_2$ | −14.52 | −14.63 | −14.75 | −14.87 | −14.99 | d |
| H | C | −14.78 | −14.90 | −15.02 | −15.14 | −15.25 | d | CN | $N_2$ | −14.53 | −14.65 | −14.77 | −14.89 | −15.01 | d |
| H | O | −14.79 | −14.91 | −15.03 | −15.15 | −15.26 | d | CN | CN | −14.52 | −14.64 | −14.76 | −14.88 | −15.00 | d |
| H | N | −14.73 | −14.81 | −14.91 | −15.06 | −15.27 | a | NO | C | −14.63 | −14.75 | −14.87 | −14.99 | −15.11 | d |
| H | H | −14.83 | −14.93 | −15.06 | −15.20 | −15.39 | e | NO | H | −14.71 | −14.83 | −14.95 | −15.07 | −15.19 | d |
| CO | C | −14.62 | −14.74 | −14.86 | −14.98 | −15.10 | d | NO | CO | −14.56 | −14.68 | −14.80 | −14.92 | −15.04 | d |
| CO | O | −14.62 | −14.74 | −14.86 | −14.98 | −15.10 | d | NO | $C_2$ | −14.54 | −14.66 | −14.78 | −14.90 | −15.01 | d |
| CO | N | −14.60 | −14.72 | −14.84 | −14.96 | −15.08 | d | NO | CN | −14.55 | −14.67 | −14.78 | −14.90 | −15.02 | d |
| CO | H | −14.70 | −14.82 | −14.94 | −15.06 | −15.18 | d | $O_2$ | C | −14.64 | −14.76 | −14.88 | −15.00 | −15.12 | d |
| CO | CO | −14.55 | −14.67 | −14.79 | −14.91 | −15.02 | d | $O_2$ | H | −14.73 | −14.85 | −14.97 | −15.08 | −15.20 | d |
| $C_2$ | C | −14.60 | −14.72 | −14.84 | −14.95 | −15.07 | d | $O_2$ | CO | −14.57 | −14.69 | −14.81 | −14.93 | −15.05 | d |
| $C_2$ | O | −14.60 | −14.72 | −14.84 | −14.96 | −15.08 | d | $O_2$ | $C_2$ | −14.55 | −14.67 | −14.79 | −14.91 | −15.02 | d |
| $C_2$ | N | −14.58 | −14.70 | −14.82 | −14.94 | −15.06 | d | $O_2$ | CN | −14.56 | −14.68 | −14.80 | −14.91 | −15.03 | d |
| $C_2$ | H | −14.68 | −14.80 | −14.91 | −15.03 | −15.15 | d | $H_2$ | C | −14.75 | −14.87 | −14.98 | −15.10 | −15.22 | d |
| $C_2$ | CO | −14.53 | −14.65 | −14.77 | −14.88 | −15.00 | d | $H_2$ | O | −14.76 | −14.87 | −14.99 | −15.11 | −15.23 | d |
| $C_2$ | $C_2$ | −14.51 | −14.63 | −14.75 | −14.86 | −14.98 | d | $H_2$ | N | −14.73 | −14.85 | −14.97 | −15.09 | −15.21 | d |
| $N_2$ | C | −14.62 | −14.73 | −14.85 | −14.97 | −15.09 | d | $H_2$ | H | −14.94 | −15.08 | −15.26 | −15.46 | −15.67 | a |
| $N_2$ | H | −14.72 | −14.84 | −15.01 | −15.18 | −15.35 | a | $H_2$ | CO | −14.67 | −14.79 | −14.91 | −15.03 | −15.15 | d |
| $N_2$ | CO | −14.54 | −14.66 | −14.78 | −14.90 | −15.02 | d | $H_2$ | $C_2$ | −14.65 | −14.77 | −14.88 | −15.00 | −15.12 | d |
| $N_2$ | $C_2$ | −14.52 | −14.64 | −14.76 | −14.88 | −15.00 | d | $H_2$ | $N_2$ | −14.66 | −14.78 | −14.90 | −15.02 | −15.14 | d |

**(Continued)**

**Table 2 Common logarithm of the collision integrals $\pi\Omega^{(2,2)}$ excluding collision pairs listed in Ref. 14 (continued)**

| Collision pair | | T 2,000 | 4,000 | 8,000 | 16,000 | 32,000 | Method | Collision pair | | T 2,000 | 4,000 | 8,000 | 16,000 | 32,000 | Method |
|---|---|---|---|---|---|---|---|---|---|---|---|---|---|---|---|
| $H_2$ | CN | −14.66 | −14.77 | −14.89 | −15.01 | −15.13 | d | $H^+$ | $H^+$ | −11.50 | −12.10 | −12.70 | −13.30 | −13.78 | f |
| $H_2$ | NO | −14.68 | −14.80 | −14.92 | −15.04 | −15.16 | d | $O^+$ | C | −14.38 | −14.50 | −14.62 | −14.74 | −14.86 | c |
| $H_2$ | $O_2$ | −14.70 | −14.82 | −14.93 | −15.05 | −15.17 | d | $O^+$ | O | −14.56 | −14.66 | −14.78 | −14.92 | −15.07 | a |
| $H_2$ | $H_2$ | −14.82 | −14.87 | −14.97 | −15.11 | −15.31 | e | $O^+$ | N | −14.55 | −14.64 | −14.72 | −14.86 | −15.03 | a |
| $C_3$ | C | −14.62 | −14.74 | −14.86 | −14.98 | −15.10 | d | $O^+$ | H | −14.38 | −14.50 | −14.62 | −14.74 | −14.86 | c |
| $C_3$ | O | −14.62 | −14.75 | −14.86 | −14.98 | −15.10 | d | $O^+$ | CO | −14.38 | −14.50 | −14.62 | −14.74 | −14.86 | c |
| $C_3$ | N | −14.60 | −14.72 | −14.84 | −14.96 | −15.08 | d | $O^+$ | $C_2$ | −14.38 | −14.50 | −14.62 | −14.74 | −14.86 | c |
| $C_3$ | H | −14.71 | −14.83 | −14.95 | −15.07 | −15.18 | d | $O^+$ | CN | −14.38 | −14.50 | −14.62 | −14.74 | −14.86 | c |
| $C_3$ | CO | −14.55 | −14.67 | −14.79 | −14.90 | −15.02 | d | $O^+$ | $H_2$ | −14.38 | −14.50 | −14.62 | −14.74 | −14.86 | c |
| $C_3$ | $C_2$ | −14.52 | −14.64 | −14.76 | −14.88 | −15.00 | d | $O^+$ | $C_3$ | −14.38 | −14.50 | −14.62 | −14.74 | −14.86 | c |
| $C_3$ | $N_2$ | −14.54 | −14.66 | −14.78 | −14.90 | −15.02 | d | $O^+$ | $C_2H$ | −14.38 | −14.50 | −14.62 | −14.74 | −14.86 | c |
| $C_3$ | CN | −14.53 | −14.65 | −14.77 | −14.89 | −15.01 | d | $O^+$ | $C^+$ | −11.50 | −12.10 | −12.70 | −13.30 | −13.78 | f |
| $C_3$ | NO | −14.56 | −14.68 | −14.80 | −14.92 | −15.03 | d | $O^+$ | $H^+$ | −11.50 | −12.10 | −12.70 | −13.30 | −13.78 | f |
| $C_3$ | $O_2$ | −14.57 | −14.69 | −14.81 | −14.93 | −15.05 | d | $N^+$ | C | −14.38 | −14.50 | −14.62 | −14.74 | −14.86 | c |
| $C_3$ | $H_2$ | −14.68 | −14.80 | −14.91 | −15.03 | −15.15 | d | $N^+$ | O | −14.57 | −14.67 | −14.81 | −14.97 | −15.13 | a |
| $C_3$ | $C_3$ | −14.53 | −14.66 | −14.79 | −14.91 | −15.03 | d | $N^+$ | N | −14.48 | −14.58 | −14.69 | −14.85 | −15.06 | a |
| $C_2H$ | C | −14.62 | −14.74 | −14.86 | −14.98 | −15.10 | d | $N^+$ | H | −14.38 | −14.50 | −14.62 | −14.74 | −14.86 | c |
| $C_2H$ | O | −14.62 | −14.75 | −14.86 | −14.98 | −15.10 | d | $N^+$ | CO | −14.38 | −14.50 | −14.62 | −14.74 | −14.86 | c |
| $C_2H$ | N | −14.60 | −14.72 | −14.84 | −14.96 | −15.08 | d | $N^+$ | $C_2$ | −14.38 | −14.50 | −14.62 | −14.74 | −14.86 | c |
| $C_2H$ | H | −14.71 | −14.83 | −14.95 | −15.07 | −15.18 | d | $N^+$ | CN | −14.38 | −14.50 | −14.62 | −14.74 | −14.86 | c |
| $C_2H$ | CO | −14.55 | −14.67 | −14.79 | −14.90 | −15.02 | d | $N^+$ | $H_2$ | −14.38 | −14.50 | −14.62 | −14.74 | −14.86 | c |
| $C_2H$ | $C_2$ | −14.52 | −14.64 | −14.76 | −14.88 | −15.00 | d | $N^+$ | $C_3$ | −14.38 | −14.50 | −14.62 | −14.74 | −14.86 | c |
| $C_2H$ | $N_2$ | −14.54 | −14.66 | −14.78 | −14.90 | −15.02 | d | $N^+$ | $C_2H$ | −14.38 | −14.50 | −14.62 | −14.74 | −14.86 | c |
| $C_2H$ | CN | −14.53 | −14.65 | −14.77 | −14.89 | −15.01 | d | $N^+$ | $C^+$ | −11.50 | −12.10 | −12.70 | −13.30 | −13.78 | f |
| $C_2H$ | NO | −14.56 | −14.68 | −14.80 | −14.92 | −15.04 | d | $N^+$ | $H^+$ | −11.50 | −12.10 | −12.70 | −13.30 | −13.78 | f |
| $C_2H$ | $O_2$ | −14.57 | −14.69 | −14.81 | −14.93 | −15.05 | d | $NO^+$ | C | −14.38 | −14.50 | −14.62 | −14.74 | −14.86 | c |
| $C_2H$ | $H_2$ | −14.68 | −14.80 | −14.91 | −15.03 | −15.15 | d | $NO^+$ | H | −14.38 | −14.50 | −14.62 | −14.74 | −14.86 | c |
| $C_2H$ | $C_3$ | −14.53 | −14.66 | −14.79 | −14.91 | −15.03 | d | $NO^+$ | CO | −14.38 | −14.50 | −14.62 | −14.74 | −14.86 | c |
| $C_2H$ | $C_2H$ | −14.53 | −14.67 | −14.79 | −14.91 | −15.03 | d | $NO^+$ | $C_2$ | −14.38 | −14.50 | −14.62 | −14.74 | −14.86 | c |
| $C^+$ | C | −14.38 | −14.50 | −14.62 | −14.74 | −14.86 | c | $NO^+$ | CN | −14.38 | −14.50 | −14.62 | −14.74 | −14.86 | c |
| $C^+$ | O | −14.38 | −14.50 | −14.62 | −14.74 | −14.86 | c | $NO^+$ | $H_2$ | −14.38 | −14.50 | −14.62 | −14.74 | −14.86 | c |
| $C^+$ | N | −14.38 | −14.50 | −14.62 | −14.74 | −14.86 | c | $NO^+$ | $C_3$ | −14.38 | −14.50 | −14.62 | −14.74 | −14.86 | c |
| $C^+$ | H | −14.38 | −14.50 | −14.62 | −14.74 | −14.86 | c | $NO^+$ | $C_2H$ | −14.38 | −14.50 | −14.62 | −14.74 | −14.86 | c |
| $C^+$ | CO | −14.38 | −14.50 | −14.62 | −14.74 | −14.86 | c | $NO^+$ | $C^+$ | −11.50 | −12.10 | −12.70 | −13.30 | −13.78 | f |
| $C^+$ | $C_2$ | −14.45 | −14.56 | −14.68 | −14.80 | −14.92 | d | $NO^+$ | $H^+$ | −11.50 | −12.10 | −12.70 | −13.30 | −13.78 | f |
| $C^+$ | $N_2$ | −14.38 | −14.50 | −14.62 | −14.74 | −14.86 | c | $N_2^+$ | C | −14.38 | −14.50 | −14.62 | −14.74 | −14.86 | c |
| $C^+$ | CN | −14.38 | −14.50 | −14.62 | −14.74 | −14.86 | c | $N_2^+$ | H | −14.38 | −14.50 | −14.62 | −14.74 | −14.86 | c |
| $C^+$ | NO | −14.38 | −14.50 | −14.62 | −14.74 | −14.86 | c | $N_2^+$ | CO | −14.38 | −14.50 | −14.62 | −14.74 | −14.86 | c |
| $C^+$ | $O_2$ | −14.38 | −14.50 | −14.62 | −14.74 | −14.86 | c | $N_2^+$ | $C_2$ | −14.38 | −14.50 | −14.62 | −14.74 | −14.86 | c |
| $C^+$ | $H_2$ | −14.38 | −14.50 | −14.62 | −14.74 | −14.86 | c | $N_2^+$ | CN | −14.38 | −14.50 | −14.62 | −14.74 | −14.86 | c |
| $C^+$ | $C_3$ | −14.38 | −14.50 | −14.62 | −14.74 | −14.86 | c | $N_2^+$ | $H_2$ | −14.38 | −14.50 | −14.62 | −14.74 | −14.86 | c |
| $C^+$ | $C_2H$ | −14.38 | −14.50 | −14.62 | −14.74 | −14.86 | c | $N_2^+$ | $C_3$ | −14.38 | −14.50 | −14.62 | −14.74 | −14.86 | c |
| $C^+$ | $C^+$ | −11.50 | −12.10 | −12.70 | −13.30 | −13.78 | f | $N_2^+$ | $C_2H$ | −14.38 | −14.50 | −14.62 | −14.74 | −14.86 | c |
| $H^+$ | C | −14.38 | −14.50 | −14.62 | −14.74 | −14.86 | c | $N_2^+$ | $C^+$ | −11.50 | −12.10 | −12.70 | −13.30 | −13.78 | f |
| $H^+$ | O | −14.38 | −14.50 | −14.62 | −14.74 | −14.86 | c | $N_2^+$ | $H^+$ | −11.50 | −12.10 | −12.70 | −13.30 | −13.78 | f |
| $H^+$ | N | −14.38 | −14.50 | −14.62 | −14.74 | −14.86 | c | $e^-$ | C | −14.38 | −14.36 | −14.40 | −14.41 | −14.39 | b |
| $H^+$ | H | −14.25 | −14.42 | −14.61 | −14.81 | −15.19 | e | $e^-$ | O | −15.56 | −15.32 | −15.11 | −14.98 | −14.95 | b |
| $H^+$ | CO | −14.38 | −14.50 | −14.62 | −14.74 | −14.86 | c | $e^-$ | N | −14.73 | −14.62 | −14.58 | −14.54 | −14.40 | b |
| $H^+$ | $C_2$ | −14.54 | −14.66 | −14.78 | −14.90 | −15.02 | d | $e^-$ | H | −14.69 | −14.79 | −14.89 | −14.92 | −14.94 | b |
| $H^+$ | $N_2$ | −14.38 | −14.50 | −14.62 | −14.74 | −14.86 | c | $e^-$ | CO | −15.29 | −15.06 | −14.94 | −15.11 | −15.78 | g |
| $H^+$ | CN | −14.38 | −14.50 | −14.62 | −14.74 | −14.86 | c | $e^-$ | $C_2$ | −15.29 | −15.06 | −14.94 | −15.11 | −15.78 | g |
| $H^+$ | NO | −14.38 | −14.50 | −14.62 | −14.74 | −14.86 | c | $e^-$ | CN | −15.29 | −15.06 | −14.94 | −15.11 | −15.78 | g |
| $H^+$ | $O_2$ | −14.38 | −14.50 | −14.62 | −14.74 | −14.86 | c | $e^-$ | $H_2$ | −14.87 | −14.81 | −14.78 | −14.78 | −14.86 | e |
| $H^+$ | $H_2$ | −14.38 | −14.50 | −14.62 | −14.74 | −14.86 | c | $e^-$ | $C_3C3$ | −15.29 | −15.06 | −14.94 | −15.11 | −15.78 | g |
| $H^+$ | $C_3$ | −14.38 | −14.50 | −14.62 | −14.74 | −14.86 | c | $e^-$ | $C_2H$ | −15.29 | −15.06 | −14.94 | −15.11 | −15.78 | g |
| $H^+$ | $C_2H$ | −14.38 | −14.50 | −14.62 | −14.74 | −14.86 | c | $e^-$ | $C^+$ | −11.50 | −12.10 | −12.70 | −13.30 | −13.78 | f |
| $H^+$ | $C^+$ | −11.50 | −12.10 | −12.70 | −13.30 | −13.78 | f | $e^-$ | $H^+$ | −11.50 | −12.10 | −12.70 | −13.30 | −13.78 | f |

**Modified Lennard–Jones Method**

For the neutral–neutral collision pairs involving the species containing carbon or hydrogen that are not previously calculated quantum mechanically, collision integrals are derived here by modifying the Lennard–Jones (LJ) approximation. In Ref. 26, a method of estimating collision integrals is given for the case where the interaction between colliding particles is by a LJ (12–6) potential. The two characteristic quantities governing the potential, that is, the collision diameter $d$ and the attractive potential well depth $\epsilon/k$, are given in Ref. 27, among others, for C, CN, CO, $C_2$, H, $H_2$, N, $N_2$, NO, O, and $O_2$. The parameters for $C_3$ and $C_2H$ have been determined in Ref. 28 using the method given in Ref. 27. (These parameters are not explicitly given in Ref. 28, but they can be deduced from the diffusion coefficient values given therein.) The LJ parameters so chosen are presented in Table 3.

The collision integrals obtained by this method are compared with the quantum-mechanical calculations in Fig. 2. As seen in Fig. 2, the LJ approximation is slightly larger than the quantum-mechanical values at 2000 K and overestimates by a factor of about 5 at 32,000 K. The large deviation at high temperature is understandable: The LJ description accounts mostly for the effective long-range interactions dominant at lower temperatures. At high temperatures, the

**Table 3 LJ parameters and bifurcation model parameter $F_i$**

| Species | $d$, A | $\epsilon/k$, K | $F_{i,1}$ (1.0; 0.865)[a] | $F_{i,2}$ (0.1; 0.283)[a] | $F_{i,3}$ (0.01; 0.0969)[a] | $F_{i,4}$ (0.001; 0.0483)[a] |
|---|---|---|---|---|---|---|
| C | 3.385 | 30.5 | 0.3844 | 0.6163 | 0.5950 | 0.6240 |
| O | 3.050 | 106.7 | 0.5006 | 0.6426 | 0.6469 | 0.6841 |
| N | 3.298 | 71.4 | 0.5252 | 0.7238 | 0.6806 | 0.6870 |
| H | 2.708 | 37.0 | 0.1317 | 0.1990 | 0.1825 | 0.1833 |
| CO | 3.690 | 91.7 | 0.7015 | 0.9379 | 0.9152 | 0.8648 |
| $C_2$ | 3.913 | 78.8 | 0.7000 | 0.9783 | 0.9013 | 0.9268 |
| $N_2$ | 3.798 | 71.4 | 0.5751 | 1.0411 | 0.9620 | 0.9433 |
| CN | 3.856 | 75.0 | 0.5920 | 1.0213 | 0.8723 | 0.9133 |
| NO | 3.599 | 91.0 | 0.8475 | 0.9628 | 0.9732 | 0.9579 |
| $O_2$ | 3.467 | 106.7 | 0.8289 | 0.9363 | 0.9628 | 0.9731 |
| $H_2$ | 2.827 | 59.7 | 0.2204 | 0.2854 | 0.2641 | 0.2649 |
| $C_3$ | 3.245 | 535.3 | 0.9014 | 0.9487 | 0.9897 | 0.9721 |
| $C_2H$ | 3.243 | 538.0 | 0.8225 | 0.9094 | 0.9361 | 0.8931 |
| $C^+$ | | | 1.9669 | 1.4920 | 1.7979 | 1.8439 |
| $H^+$ | | | 0.6785 | 0.5420 | 0.5513 | 0.6120 |
| $O^+$ | | | 2.8809 | 2.2381 | 2.5087 | 2.6937 |
| $N^+$ | | | 2.0710 | 1.6913 | 1.8349 | 1.9702 |
| $NO^+$ | | | 2.8144 | 2.3308 | 2.5287 | 2.7152 |
| $N_2^+$ | | | 2.7690 | 2.2613 | 2.4533 | 2.6342 |
| $e^-$ | | | 2.0267 | 1.6225 | 1.7682 | 1.9552 |

[a]Weight to ions; $\log_{10}(\sigma)$.

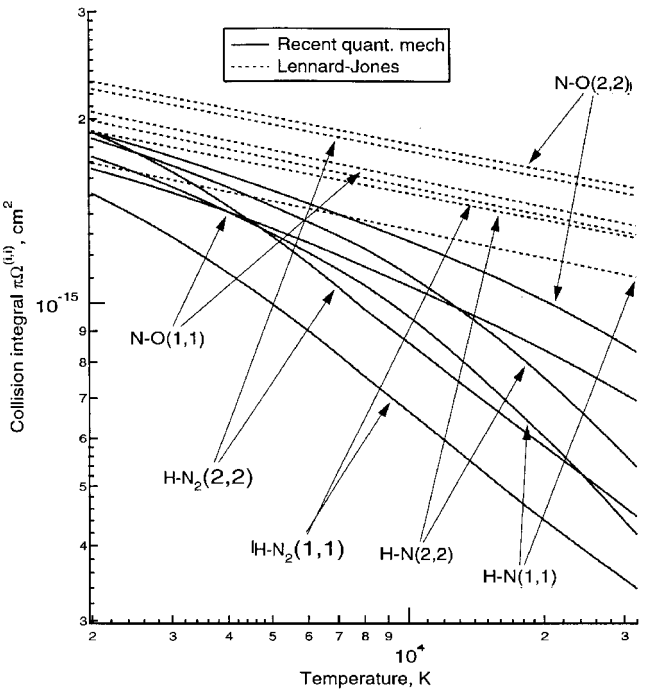


**Fig. 2 Comparison of collision integrals between the LJ approximation and recent quantum-mechanical values.**

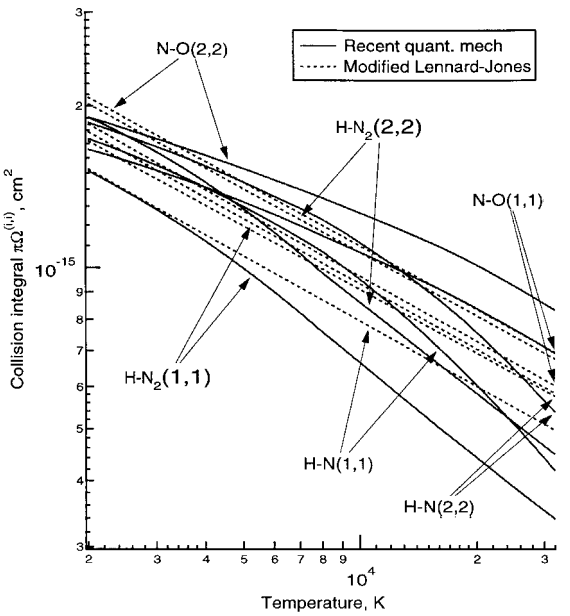


**Fig. 3 Comparison between the collision integrals obtained in recent quantum-mechanical calculations and the modified LJ approximation.**

governing potentials are very different from the LJ potential. In the present work, an arbitrary modification is made to the LJ collision integrals as

$$\Omega(\text{modified LJ}) = 0.9\Omega(\text{LJ})(T/2000)^{-0.25} \quad (1)$$

In Fig. 3 the collision integral values for the neutral–neutral collisions calculated by the modified LJ approximation are compared with the recent quantum-mechanical values. Figure 3 shows that the modified LJ approximation agrees with the quantum-mechanical values fairly well. This method is used for the neutral–neutral collisions involving the carbonaceous and hydrogeneous species. This method is named method d in Tables 1 and 2.

A more rigorous procedure for estimating the transport properties by employing the effective interaction potential with helium atom and then employing combination relations for the short-range and long-range components is under development.[21] When compared with the quantum-mechanical solutions, this method yields results that agree to within 3% (Ref. 21). The present modified LJ procedure could be replaced in the future by this method.

### Collisions Among Hydrogenic Species

For collision pairs among hydrogeneous species, Ref. 29 summarized the collision integral values known in 1962. For those collision pairs among the hydrogen species that were not calculated quantum mechanically in recent years, the values in Ref. 29 are adopted in the present work. This method is identified as method e (Tables 1 and 2).

### Coulomb Collisions

For coulomb collisions, Ref. 14 provides a detailed method of determining collision integrals as a function of electron pressure. As an approximation, a set for the electron pressure of 1 atm is selected. Because the collision integrals for coulomb collisions are very large, and therefore all ionized species tend to be locked together, this approximation probably leads to only a small error (see "Bifurcation

Model" subsection). This method is identified as method f (Tables 1 and 2).

**Electron–Neutral Collisions for Carbonaceous Species**

For electron–neutral collisions involving CO, CN, $C_2$, $C_3$, and $C_2H$, there are presently no means of determining their collision integrals. Their collision integrals are assumed to be the same as for the e–NO collisions. This method is identified as method g (Tables 1 and 2).

**Compilation of Gupta et al.[14]**

For collision pairs among oxygen and nitrogen, Gupta et al.[14] compiled the collision integrals known in 1962. In Figs. 4a and 4b, comparison is made between the recent quantum-mechanical calculations and the values given in Ref. 14. Figures 4 show that these two sets of values differ only slightly. For those collision pairs not determined by methods a–g, the values of Ref. 14 are adopted in the present work.

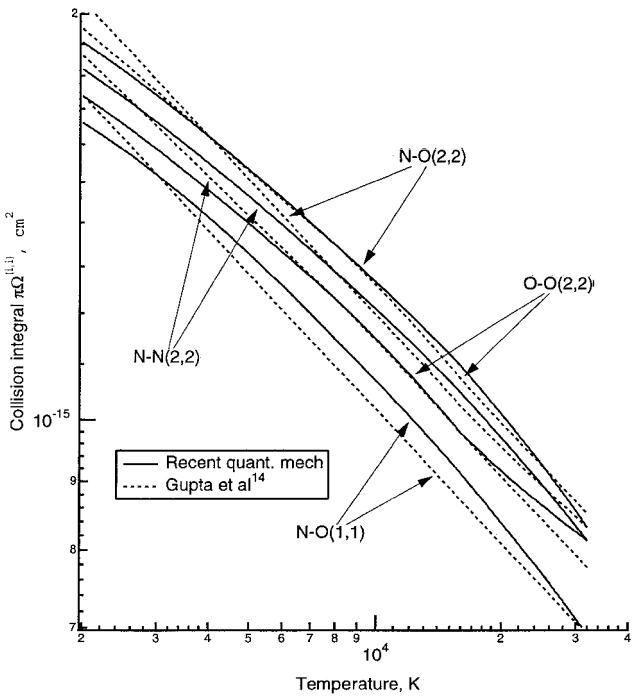


**a) Neutral–neutral collisions**

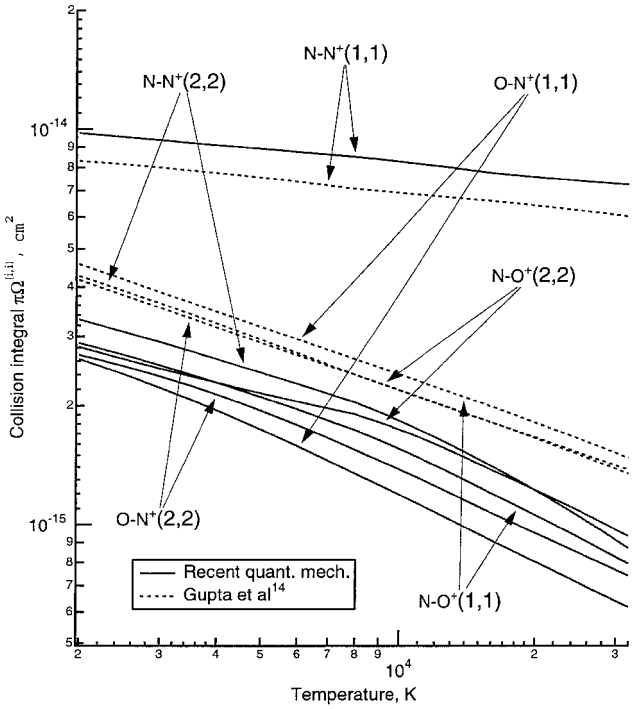


**b) Ion–neutral collisions**

**Fig. 4 Comparison of collision integrals between the recent quantum-mechanical calculations and the compilation in Ref. 14.**

**Ambipolar Diffusion**

For a three-species mixture consisting of a neutral species, its ion, and electron in a single temperature situation, the effective diffusion coefficient $D_{ef}^+$ for the ion is known to be twice that calculated from the collision integrals, that is,

$$D_{ef}^+ = 2D^+ \tag{2}$$

This is known as ambipolar diffusion effect. If the electron temperature $T_e$ is different from the heavy particle temperature $T$, this becomes[30]

$$D_{ef}^+ = (1 + T_e/T)D^+$$

In a multicomponent two-temperature mixture, a similar averaging formula is known.[30]

**Diffusion Models**

According to the well-known kinetic theory,[26] the mass flux of species $i$ by diffusion in a multicomponent mixture is expressed by

$$J_i = \rho \sum_j \frac{M_i}{\bar{M}} \frac{M_j}{\bar{M}} D_{ij} \frac{\partial X_j}{\partial y} \tag{3}$$

The coefficient of self-diffusion, $D_{ii}$, is defined to be zero in this description. In the computation of flow motion using a computational fluid dynamics (CFD) technique, the effect of diffusion of species $i$ is represented in the differential equation for species mass conservation for species $i$ in this case by a term containing the sum of the second derivatives of $X_j$ over $j$. Because $D_{ii}$ is zero, the equation for species $i$ lacks the second derivative of $X_i$. That is, the diagonal terms are missing. By a well-known principle of CFD, time integration of this equation set becomes unstable.

A slightly less unstable set can be derived by setting

$$X_j = 1 - \sum_{k \neq j} X_k$$

in Eq. (3) and changing the order of summations, which leads to

$$J_i = -\rho \sum_j \left[ \sum_{k \neq j} \frac{M_i}{\bar{M}} \frac{M_k}{\bar{M}} D_{ik} \right] \frac{\partial X_j}{\partial y}$$

Defining the quantity in the parenthesis as an effective diffusion coefficient $\bar{D}_{ij}$, one obtains

$$J_i = -\rho \sum_j \bar{D}_{ij} \frac{\partial X_j}{\partial y} \tag{4}$$

When this formulation is used, diagonal terms are finite in the differential equation set. However, the off-diagonal terms are solidly filled with values of the same magnitude as the diagonal terms. The resulting differential equation set is on the border between being stable and unstable (see "Multicomponent Diffusion Model" subsection).

An approximate method known as the bifurcation model, which leads to a stable differential equation set, was first introduced by Bird[31] and was used in Ref. 28. In that method, the binary diffusion coefficient between species $i$ and $j$ is expressed as

$$D_{ij} = \bar{D}/F_i F_j \tag{5}$$

where $\bar{D}$ is a reference self-diffusion coefficient chosen arbitrarily. If there is a unique set of $F_i$ values that makes Eq. (5) valid for all species at all temperatures, then the diffusion flux of species $i$ is

expressible with only one spatial gradient involving species $i$, in the form

$$J_i = -\frac{\rho \bar{D} \mu_2}{\bar{M} \mu_1} \frac{\partial Z_i}{\partial y} \tag{6}$$

where $Z_i$ is an equivalent species concentration

$$Z_i = M_i X_i / F_i \mu_2 \tag{7}$$

Here,

$$\mu_1 = \sum_j X_j F_j, \qquad \mu_2 = \sum_j M_j X_j / F_j \tag{8}$$

The CFD equation set based on this formulation is stable (see "Bifurcation Model" subsection).

The parameter $F_i$ must be determined through a least-square fit. That is, those values of $F_i$ must be found that make the standard deviation $\sigma$ between Eq. (5) and the true values of binary diffusion coefficient for all species combinations and all temperatures considered the smallest.[28] Depending on the purpose, different weights could be given to different collision pairs and temperatures in the evaluation of $\sigma$. In Ref. 28, it is shown that, for collisions among neutral species, a set of $F_i$ values that brings Eq. (5) to within 1% of the true values can be obtained with equal weights for all species and for all temperatures. Such a close fit resulted because all interactions were taken to be of the LJ type.

For the present set of species, the least-square fit was performed at 2500, 5000, 7500, 10,000, and 12,500 K. Even though temperature reaches much higher values in the shock layer, the upper limit of 12,500 K is considered adequate because transport phenomena are significant only in the boundary layer where temperature stays below about 12,000 K. The true binary diffusion coefficients were calculated with the collision integral values given earlier. For ions, the calculated binary diffusion coefficients were doubled according to Eq. (2) to account for the ambipolar effect. The reference self-diffusion coefficient $\bar{D}$ was taken to be that for the $N_2$–$N_2$ collision. The numerical values for $\bar{D}$ are presented in Table 4. Viscosity, the Schmidt number based on $\bar{D}$, and Prandtl number are also presented in Table 4 for the mixtures with fixed species concentrations of 79%$N_2$–21%$O_2$ and 79%N–21%O by volume for reference.

Four different weights were considered in evaluating the standard deviation $\sigma$: 1) all unity, 2) unity for all but 0.1 for collisions involving charged particles, 3) unity for all but 0.01 for collisions involving charged particles, and 4) unity for all but 0.001 for collisions involving charged particles. The standard deviation is calculated in the logarithmic scale. The four sets of $F_i$ values so obtained are named $F_{i,1}$–$F_{i,4}$, respectively. In Table 3, the $F_i$ values and the logarithm of the standard deviation $\sigma$ for these four cases are presented.

As seen in Table 3, an equal weight to all collisions, resulting in $F_{i,1}$, leads to a standard deviation $\sigma$ of a factor of $10^{0.865} = 7.3$. When a weight of 0.001 is given to the charge-involved collisions, $F_{i,4}$, standard deviation falls to a factor of $10^{0.0483} = 1.12$. The standard deviation for the present system tends to be larger than that considered in Ref. 28, which is understandable because the interactions in the present set are not of the LJ type. All values of $F_i$ are significantly different from those in Ref. 28. The impact of the choice of $F_i$ on the flowfield solutions will be discussed further later in the "Bifurcation Model" subsection.

**Table 4 Reference diffusion coefficient $\bar{D}$ at 1 atm, viscosity, reference Schmidt number with respect to $\bar{D}$, and Prandtl number for mixtures with fixed concentrations**

| | | $N_2$(0.79)–$O_2$(0.21) | | | N(0.79)–O(0.21) | | |
|---|---|---|---|---|---|---|---|
| $T$, K | $\bar{D}$, m²/s | $\mu$, m²/s | $\bar{S}c$ | $Pr$ | $\mu$, m²/s | $\bar{S}c$ | $Pr$ |
| 2,000 | $5.186^{-4}$ | $6.532^{-5}$ | 0.7164 | 0.9328 | $7.719^{-5}$ | 1.693 | 0.6655 |
| 4,000 | $1.805^{-3}$ | $1.048^{-4}$ | 0.6603 | 0.9300 | $1.282^{-4}$ | 1.617 | 0.6555 |
| 8,000 | $6.280^{-3}$ | $1.788^{-4}$ | 0.6477 | 0.9284 | $2.181^{-4}$ | 1.580 | 0.6555 |
| 16,000 | $2.236^{-2}$ | $3.078^{-4}$ | 0.6265 | 0.9275 | $3.798^{-4}$ | 1.546 | 0.6556 |
| 32,000 | $7.962^{-2}$ | $5.526^{-4}$ | 0.6316 | 0.9280 | $6.953^{-4}$ | 1.590 | 0.6556 |

## Chemical Reaction Rates

The chemical reactions scheme of significance and their reaction rate coefficient adopted in the present work are listed in Table 5. The forward reaction rate coefficients are expressed as

$$k_f = C T^n \exp(-T_r / T_a) \tag{9}$$

where $T_a$ is the temperature controlling the reaction. The parameters $C$, $n$, and $T_r$ are listed in Table 5. The equilibrium constants for these reactions are defined as

$$K_e = \rho(\gamma_B \gamma_C / \gamma_A)_E \tag{10}$$

for the thermal dissociation or ionization of the type $A + M \rightarrow B + C + M$, and as

$$K_e = (\gamma_C \gamma_D / \gamma_A \gamma_B)_E \tag{11}$$

for the binary reactions of the type $A + B \rightarrow C + D$. Here, density is in the units of grams per cubic centimeter and the species concentration $\gamma_i$ is in mole per gram. The equilibrium constants are calculated for these reactions at 3000, 6000, 9000, 12,000, and 15,000 K. The resulting values are fitted by an expression

$$K_e = \exp\left[A_1/Z + A_2 + A_3 \ln(Z) + A_4 Z + A_5 Z^2\right] \tag{12}$$

where $Z = 10{,}000/T$. The parameters $A_1$–$A_5$ for the reactions are presented in Table 6.

The sources of the rate parameters in Table 5 are from Refs. 32–37, except for the six reactions newly chosen in the present work, reactions 9, 10, and 19–22. The electron-impact ionization rates for C and H, reactions 9 and 10, are deduced from the measured ionic recombination rates for $H^+$, $H_e^+$, $C^+$, and $N^+$ (Refs. 38–42). In Fig. 5, the expressions adopted in the present work are compared with the experimental data. As seen in Fig. 5, the chosen expressions represent a good fit to the experimental data.

There are four four-body reactions, $CO + C_2 \rightarrow C_3 + O$, $C_3 + N \rightarrow CN + C_2$, $C_3 + C \rightarrow C_2 + C_2$, and $C_2H + H \rightarrow C_2 + H_2$, reactions 19–22, for which the rate parameters are unknown. For these reactions, $n$ was assumed to be zero and $T_r$ was assumed to be that corresponding to the energy of reaction. Then $C$ was estimated by comparing with the $C$ value for the reactions $N + CO_2 \rightarrow NO + CO$, $N + O_3 \rightarrow NO + O_2$, $N + NO_2 \rightarrow N_2O + O$, $N + NO_2 \rightarrow NO + NO$, $O + CO_2 \rightarrow O_2 + CO$, and $H + HNO \rightarrow OH + NH$ (Ref. 43), which resemble the reactions in question. The $C$ values for these known reactions are between about $10^{11}$ and $3 \times 10^{12}$ cm³/(mol · s). Therefore, the $C$ value for reactions 19–22 are taken to be $10^{12}$ cm³/(mol · s). The impact of this choice will be examined later in the "Sample Flowfield Calculation" section.

## Surface Reactions

### Surface Mass Balance

In past analyses, gas–surface reaction was assumed to be in equilibrium (e.g., see Ref. 44). In recent years, it became apparent that, at least for the Earth entries of present interest, the flow over an entry body is not in thermochemical equilibrium. Even for such an environment, gas–surface equilibrium has been assumed.[45,46] A calculation procedure assuming gas–surface equilibrium, named fully implicit ablation and thermal response (FIAT), has been developed.[46]

In a nonequilibrium boundary-layer flow, the slope of species concentration with respect to distance $y$ at the wall is in general finite. The finite slope produces a finite flux of the species transported by diffusion. The surface may cause chemical change to the species, thereby reducing or increasing its wall slope. In addition, the pyrolysis gas emerging from the surface may also contain the species. Mass conservation dictates that these fluxes are related by

mass flux of species $i$ in pyrolysis gas

+ mass flux of species $i$ produced at surface

= mass flux of species $i$ leaving wall

+ mass flux of species $i$ removed by diffusion (13)

**Table 5 Reaction rate coefficients, $k_f = CT^n \exp(-T_r/T)$**

| Reaction | $M$ | $C$ | $n$ | $T_r$ | $T_a$ | Reference |
|---|---|---|---|---|---|---|
| 1) $N_2 + M \rightarrow N + N + M$ | | | | | | |
| | C | $3.0^{22}$ | −1.6 | 113,200 | $\sqrt{TT_v}$ | Park[32] |
| | O | $3.0^{22}$ | −1.6 | 113,200 | $\sqrt{TT_v}$ | Park[32] |
| | N | $3.0^{22}$ | −1.6 | 113,200 | $\sqrt{TT_v}$ | Park[32] |
| | H | $3.0^{22}$ | −1.6 | 113,200 | $\sqrt{TT_v}$ | Park[32] |
| | CO | $7.0^{21}$ | −1.6 | 113,200 | $\sqrt{TT_v}$ | Park[32] |
| | $C_2$ | $7.0^{21}$ | −1.6 | 113,200 | $\sqrt{TT_v}$ | Park[32] |
| | $N_2$ | $7.0^{21}$ | −1.6 | 113,200 | $\sqrt{TT_v}$ | Park[32] |
| | CN | $7.0^{21}$ | −1.6 | 113,200 | $\sqrt{TT_v}$ | Park[32] |
| | NO | $7.0^{21}$ | −1.6 | 113,200 | $\sqrt{TT_v}$ | Park[32] |
| | CH | $7.0^{21}$ | −1.6 | 113,200 | $\sqrt{TT_v}$ | Park[32] |
| | OH | $7.0^{21}$ | −1.6 | 113,200 | $\sqrt{TT_v}$ | Park[32] |
| | $O_2$ | $7.0^{21}$ | −1.6 | 113,200 | $\sqrt{TT_v}$ | Park[32] |
| | $H_2$ | $7.0^{21}$ | −1.6 | 113,200 | $\sqrt{TT_v}$ | Park[32] |
| | $C_3$ | $7.0^{21}$ | −1.6 | 113,200 | $\sqrt{TT_v}$ | Park[32] |
| | $C_2H$ | $7.0^{21}$ | −1.6 | 113,200 | $\sqrt{TT_v}$ | Park[32] |
| | $C^+$ | $7.0^{21}$ | −1.6 | 113,200 | $\sqrt{TT_v}$ | Park[32] |
| | $H^+$ | $7.0^{21}$ | −1.6 | 113,200 | $\sqrt{TT_v}$ | Park[32] |
| | $O^+$ | $7.0^{21}$ | −1.6 | 113,200 | $\sqrt{TT_v}$ | Park[32] |
| | $N^+$ | $7.0^{21}$ | −1.6 | 113,200 | $\sqrt{TT_v}$ | Park[32] |
| | $NO^+$ | $7.0^{21}$ | −1.6 | 113,200 | $\sqrt{TT_v}$ | Park[32] |
| | $N_2^+$ | $7.0^{21}$ | −1.6 | 113,200 | $\sqrt{TT_v}$ | Park[32] |
| 2) $O_2 + M \rightarrow O + O + M$ | | | | | | |
| | C | $1.0^{22}$ | −1.5 | 59,360 | $\sqrt{TT_v}$ | Park[32] |
| | O | $1.0^{22}$ | −1.5 | 59,360 | $\sqrt{TT_v}$ | Park[32] |
| | N | $1.0^{22}$ | −1.5 | 59,360 | $\sqrt{TT_v}$ | Park[32] |
| | H | $1.0^{22}$ | −1.5 | 59,360 | $\sqrt{TT_v}$ | Park[32] |
| | CO | $2.0^{21}$ | −1.5 | 59,360 | $\sqrt{TT_v}$ | Park[32] |
| | $C_2$ | $2.0^{21}$ | −1.5 | 59,360 | $\sqrt{TT_v}$ | Park[32] |
| | $N_2$ | $2.0^{21}$ | −1.5 | 59,360 | $\sqrt{TT_v}$ | Park[32] |
| | CN | $2.0^{21}$ | −1.5 | 59,360 | $\sqrt{TT_v}$ | Park[32] |
| | NO | $2.0^{21}$ | −1.5 | 59,360 | $\sqrt{TT_v}$ | Park[32] |
| | CH | $2.0^{21}$ | −1.5 | 59,360 | $\sqrt{TT_v}$ | Park[32] |
| | OH | $2.0^{21}$ | −1.5 | 59,360 | $\sqrt{TT_v}$ | Park[32] |
| | $O_2$ | $2.0^{21}$ | −1.5 | 59,360 | $\sqrt{TT_v}$ | Park[32] |
| | $H_2$ | $2.0^{21}$ | −1.5 | 59,360 | $\sqrt{TT_v}$ | Park[32] |
| | $C_3$ | $2.0^{21}$ | −1.5 | 59,360 | $\sqrt{TT_v}$ | Park[32] |
| | $C_2H$ | $2.0^{21}$ | −1.5 | 59,360 | $\sqrt{TT_v}$ | Park[32] |
| | $C^+$ | $2.0^{21}$ | −1.5 | 59,360 | $\sqrt{TT_v}$ | Park[32] |
| | $H^+$ | $2.0^{21}$ | −1.5 | 59,360 | $\sqrt{TT_v}$ | Park[32] |
| | $O^+$ | $2.0^{21}$ | −1.5 | 59,360 | $\sqrt{TT_v}$ | Park[32] |
| | $N^+$ | $2.0^{21}$ | −1.5 | 59,360 | $\sqrt{TT_v}$ | Park[32] |
| | $NO^+$ | $2.0^{21}$ | −1.5 | 59,360 | $\sqrt{TT_v}$ | Park[32] |
| | $N_2^+$ | $2.0^{21}$ | −1.5 | 59,360 | $\sqrt{TT_v}$ | Park[32] |
| 3) $C_2 + M \rightarrow C + C + M$ | | | | | | |
| | C | $3.7^{14}$ | 0 | 69,900 | $\sqrt{TT_v}$ | Park et al.[33] |
| | O | $3.7^{14}$ | 0 | 69,900 | $\sqrt{TT_v}$ | Park et al.[33] |
| | N | $3.7^{14}$ | 0 | 69,900 | $\sqrt{TT_v}$ | Park et al.[33] |
| | H | $3.7^{14}$ | 0 | 69,900 | $\sqrt{TT_v}$ | Park et al.[33] |
| | CO | $3.7^{14}$ | 0 | 69,900 | $\sqrt{TT_v}$ | Park et al.[33] |
| | $C_2$ | $3.7^{14}$ | 0 | 69,900 | $\sqrt{TT_v}$ | Park et al.[33] |
| | $N_2$ | $3.7^{14}$ | 0 | 69,900 | $\sqrt{TT_v}$ | Park et al.[33] |
| | CN | $3.7^{14}$ | 0 | 69,900 | $\sqrt{TT_v}$ | Park et al.[33] |
| | NO | $3.7^{14}$ | 0 | 69,900 | $\sqrt{TT_v}$ | Park et al.[33] |
| | $O_2$ | $3.7^{14}$ | 0 | 69,900 | $\sqrt{TT_v}$ | Park et al.[33] |
| | $H_2$ | $3.7^{14}$ | 0 | 69,900 | $\sqrt{TT_v}$ | Park et al.[33] |
| | $C_3$ | $3.7^{14}$ | 0 | 69,900 | $\sqrt{TT_v}$ | Park et al.[33] |
| | $C_2H$ | $3.7^{14}$ | 0 | 69,900 | $\sqrt{TT_v}$ | Park et al.[33] |
| | $C^+$ | $3.7^{14}$ | 0 | 69,900 | $\sqrt{TT_v}$ | Park et al.[33] |
| | $H^+$ | $3.7^{14}$ | 0 | 69,900 | $\sqrt{TT_v}$ | Park et al.[33] |
| | $O^+$ | $3.7^{14}$ | 0 | 69,900 | $\sqrt{TT_v}$ | Park et al.[33] |
| | $N^+$ | $3.7^{14}$ | 0 | 69,900 | $\sqrt{TT_v}$ | Park et al.[33] |
| | $NO^+$ | $3.7^{14}$ | 0 | 69,900 | $\sqrt{TT_v}$ | Park et al.[33] |
| | $N_2^+$ | $3.7^{14}$ | 0 | 69,900 | $\sqrt{TT_v}$ | Park et al.[33] |
| 4) $CN + M \rightarrow C + N + M$ | | | | | | |
| | C | $2.5^{14}$ | 0 | 87,740 | $\sqrt{TT_v}$ | Park et al.[33] |
| | O | $2.5^{14}$ | 0 | 87,740 | $\sqrt{TT_v}$ | Park et al.[33] |
| | N | $2.5^{14}$ | 0 | 87,740 | $\sqrt{TT_v}$ | Park et al.[33] |
| | H | $2.5^{14}$ | 0 | 87,740 | $\sqrt{TT_v}$ | Park et al.[33] |
| | CO | $2.5^{14}$ | 0 | 87,740 | $\sqrt{TT_v}$ | Park et al.[33] |
| | $C_2$ | $2.5^{14}$ | 0 | 87,740 | $\sqrt{TT_v}$ | Park et al.[33] |
| | $N_2$ | $2.5^{14}$ | 0 | 87,740 | $\sqrt{TT_v}$ | Park et al.[33] |
| | CN | $2.5^{14}$ | 0 | 87,740 | $\sqrt{TT_v}$ | Park et al.[33] |
| | NO | $2.5^{14}$ | 0 | 87,740 | $\sqrt{TT_v}$ | Park et al.[33] |
| | $O_2$ | $2.5^{14}$ | 0 | 87,740 | $\sqrt{TT_v}$ | Park et al.[33] |
| | $H_2$ | $2.5^{14}$ | 0 | 87,740 | $\sqrt{TT_v}$ | Park et al.[33] |
| | $C_3$ | $2.5^{14}$ | 0 | 87,740 | $\sqrt{TT_v}$ | Park et al.[33] |
| | $C_2H$ | $2.5^{14}$ | 0 | 87,740 | $\sqrt{TT_v}$ | Park et al.[33] |
| | $C^+$ | $2.5^{14}$ | 0 | 87,740 | $\sqrt{TT_v}$ | Park et al.[33] |
| | $H^+$ | $2.5^{14}$ | 0 | 87,740 | $\sqrt{TT_v}$ | Park et al.[33] |
| | $O^+$ | $2.5^{14}$ | 0 | 87,740 | $\sqrt{TT_v}$ | Park et al.[33] |
| | $N^+$ | $2.5^{14}$ | 0 | 87,740 | $\sqrt{TT_v}$ | Park et al.[33] |
| | $NO^+$ | $2.5^{14}$ | 0 | 87,740 | $\sqrt{TT_v}$ | Park et al.[33] |
| | $N_2^+$ | $2.5^{14}$ | 0 | 87,740 | $\sqrt{TT_v}$ | Park et al.[33] |
| 5) $H_2 + M \rightarrow H + H + M$ | | | | | | |
| | C | $2.2^{14}$ | 0 | 48,300 | $\sqrt{TT_v}$ | Baulch et al.[34] |
| | O | $2.2^{14}$ | 0 | 48,300 | $\sqrt{TT_v}$ | Baulch et al.[34] |
| | N | $2.2^{14}$ | 0 | 48,300 | $\sqrt{TT_v}$ | Baulch et al.[34] |
| | H | $2.2^{14}$ | 0 | 48,300 | $\sqrt{TT_v}$ | Baulch et al.[34] |
| | CO | $2.2^{14}$ | 0 | 48,300 | $\sqrt{TT_v}$ | Baulch et al.[34] |
| | $C_2$ | $2.2^{14}$ | 0 | 48,300 | $\sqrt{TT_v}$ | Baulch et al.[34] |
| | $N_2$ | $2.2^{14}$ | 0 | 48,300 | $\sqrt{TT_v}$ | Baulch et al.[34] |
| | CN | $2.2^{14}$ | 0 | 48,300 | $\sqrt{TT_v}$ | Baulch et al.[34] |
| | NO | $2.2^{14}$ | 0 | 48,300 | $\sqrt{TT_v}$ | Baulch et al.[34] |
| | $O_2$ | $2.2^{14}$ | 0 | 48,300 | $\sqrt{TT_v}$ | Baulch et al.[34] |
| | $H_2$ | $5.5^{14}$ | 0 | 48,300 | $\sqrt{TT_v}$ | Oldenborg et al.[35] |
| | $C_3$ | $2.2^{14}$ | 0 | 48,300 | $\sqrt{TT_v}$ | Baulch et al.[34] |
| | $C_2H$ | $2.2^{14}$ | 0 | 48,300 | $\sqrt{TT_v}$ | Baulch et al.[34] |
| | $C^+$ | $2.2^{14}$ | 0 | 48,300 | $\sqrt{TT_v}$ | Baulch et al.[34] |
| | $H^+$ | $2.2^{14}$ | 0 | 48,300 | $\sqrt{TT_v}$ | Baulch et al.[34] |
| | $O^+$ | $2.2^{14}$ | 0 | 48,300 | $\sqrt{TT_v}$ | Baulch et al.[34] |
| | $N^+$ | $2.2^{14}$ | 0 | 48,300 | $\sqrt{TT_v}$ | Baulch et al.[34] |
| | $NO^+$ | $2.2^{14}$ | 0 | 48,300 | $\sqrt{TT_v}$ | Baulch et al.[34] |
| | $N_2^+$ | $2.2^{14}$ | 0 | 48,300 | $\sqrt{TT_v}$ | Baulch et al.[34] |
| 6) $N_2 + e^- \rightarrow N + N + e^-$ | | $3^{24}$ | −1.60 | 113,200 | $T_e$ | Park[32] |
| 7) $O + e^- \rightarrow O^+ + e^- + e^-$ | | $3.9^{33}$ | −3.78 | 158,500 | $T_e$ | Park[32] |
| 8) $N + e^- \rightarrow N^+ + e^- + e^-$ | | $2.5^{34}$ | −3.82 | 168,200 | $T_e$ | Park[32] |
| 9) $C + e^- \rightarrow C^+ + e^- + e^-$ | | $3.7^{31}$ | −3.00 | 130,720 | $T_e$ | This work |
| 10) $H + e^- \rightarrow H^+ + e^- + e^-$ | | $2.2^{30}$ | −2.80 | 157,800 | $T_e$ | This work |
| 11) $N_2 + O \rightarrow NO + N$ | | $5.7^{12}$ | 0.42 | 42,938 | $T$ | Bose and Candler[36] |
| 12) $NO + O \rightarrow O_2 + N$ | | $8.4^{12}$ | 0 | 19,400 | $T$ | Bose and Candler[37] |
| 13) $CO + C \rightarrow C_2 + O$ | | $2.0^{17}$ | −1 | 58,000 | $T$ | Park et al.[33] |
| 14) $CO + O \rightarrow O_2 + C$ | | $3.9^{13}$ | −0.18 | 69,200 | $T$ | Park et al.[33] |
| 15) $CO + N \rightarrow CN + O$ | | $1.0^{14}$ | 0 | 38,600 | $T$ | Park et al.[33] |
| 16) $N_2 + C \rightarrow CN + N$ | | $1.1^{14}$ | −0.11 | 23,200 | $T$ | Park et al.[33] |
| 17) $CN + O \rightarrow NO + C$ | | $1.6^{13}$ | 0.1 | 14,600 | $T$ | Park et al.[33] |
| 18) $CN + C \rightarrow C_2 + N$ | | $5.0^{13}$ | 0 | 13,000 | $T$ | Park et al.[33] |
| 19) $CO + C_2 \rightarrow C_3 + O$ | | $1.0^{12}$ | 0 | 41,200 | $T$ | This work |
| 20) $C_3 + N \rightarrow CN + C_2$ | | $1.0^{12}$ | 0 | 34,200 | $T$ | This work |
| 21) $C_3 + C \rightarrow C_2 + C_2$ | | $1.0^{12}$ | 0 | 16,400 | $T$ | This work |
| 22) $C_2H + H \rightarrow C_2 + H_2$ | | $1.0^{12}$ | 0 | 16,770 | $T$ | This work |
| 23) $O + N \rightarrow NO^+ + e^-$ | | $5.3^{12}$ | 0 | 31,900 | $T$ | Park[32] |
| 24) $N + N \rightarrow N_2^+ + e^-$ | | $4.4^{7}$ | 1.5 | 67,500 | $T$ | Park[32] |

**Table 6 Parameters for equilibrium constant**

| $A_1$ | $A_2$ | $A_3$ | $A_4$ | $A_5$ |
|---|---|---|---|---|
| | | 1) $N_2+M=N+N+M$ | | |
| −3.293682 | 0.998998 | −8.237028 | −5.526183 | −0.582174 |
| | | 2) $O_2+M=O+O+M$ | | |
| 1.578640 | 2.688744 | 4.215573 | −8.091354 | 0.174260 |
| | | 3) $C_2+M=C+C+M$ | | |
| 2.538863 | 1.782394 | 5.753987 | −10.296164 | 0.296264 |
| | | 4) $CN+M=C+N+M$ | | |
| 1.360714 | 0.958930 | 2.726324 | −9.879787 | 0.044408 |
| | | 5) $H_2+M=H+H+M$ | | |
| 1.817328 | 1.202335 | 4.427498 | −7.574115 | 0.185211 |
| | | 6) $N_2+e^-=N+N+e^-$ | | |
| −3.293682 | 0.998998 | −8.237028 | −5.526183 | −0.582174 |
| | | 7) $O+e^-=O^+ +e^-$ | | |
| 0.614124 | −6.755241 | −0.774319 | −16.003456 | 0.005502 |
| | | 8) $N+e^-=N^+ +e^- +e^-$ | | |
| 0.200588 | −3.965871 | −0.041731 | −18.063001 | 0.125939 |
| | | 9) $C+e^-=C^+ +e^- +e^-$ | | |
| −0.283680 | −6.040219 | −1.824398 | −12.789612 | −0.036117 |
| | | 10) $H+e^-=H^+ +e^- +e^-$ | | |
| −0.192097 | −6.276289 | −1.903784 | −15.510915 | −0.025936 |
| | | 11) $N_2+O=NO+N$ | | |
| −3.032189 | 0.078468 | −7.693047 | 1.411299 | −0.517448 |
| | | 12) $NO+O=O_2+N$ | | |
| −1.840133 | −1.768215 | −4.759554 | 1.153872 | −0.238985 |
| | | 13) $CO+C=C_2+O$ | | |
| −2.294357 | 1.852541 | −5.069929 | −2.926134 | −0.268345 |
| | | 14) $CO+O=O_2+C$ | | |
| −1.334134 | 0.946191 | −3.531516 | −5.130943 | −0.146341 |
| | | 15) $CO+N=CN+O$ | | |
| −1.116209 | 2.676006 | −2.042267 | −3.342510 | −0.016489 |
| | | 16) $N_2+C=CN+N$ | | |
| −4.654396 | 0.040068 | −10.963353 | 4.353604 | −0.626582 |
| | | 17) $CN+O=NO+C$ | | |
| 1.622207 | 0.038401 | 3.270306 | −2.942305 | 0.109134 |
| | | 18) $CN+C=C2+N$ | | |
| −1.178148 | −0.823465 | −3.027662 | 0.416377 | −0.251856 |
| | | 19) $CO+C_2=C_3+O$ | | |
| 3.948366 | −2.399362 | 1.776403 | −4.373308 | −0.036555 |
| | | 20) $C_3+N=CN+C_2$ | | |
| −5.899394 | 5.259174 | −5.060829 | 1.734790 | −0.034435 |
| | | 21) $C_3+C=C_2+C_2$ | | |
| −4.340555 | 4.842954 | −2.825133 | −1.197910 | 0.035351 |
| | | 22) $C_2H+H=C_2+H_2$ | | |
| 2.548009 | −1.020366 | 3.425799 | −1.864180 | 0.071191 |
| | | 23) $O+N=NO^+ +e^-$ | | |
| 3.429239 | −7.431449 | 6.012721 | −8.276563 | 0.503539 |
| | | 24) $N+N=N_2^+ +e^-$ | | |
| −0.062523 | −5.822935 | −0.924052 | −8.136642 | 0.188105 |

When the bifurcation model [Eq. (6)] is used, Eq. (13) becomes

$$\dot{m}_p z_i + \dot{m}_{w,i} = \rho_w v_w z_i - \frac{\rho \bar{D} \mu_2}{\bar{M} \mu_1} \frac{\partial Z_i}{\partial y} \tag{14}$$

To contrast with the equilibrium wall condition, this relationship will be called the kinetic wall condition.

The total mass flux is related to pyrolysis rate and surface reaction rate by

$$\rho_w v_w = \dot{m}_p + \sum_i \dot{m}_{w,i} \tag{15}$$

Because of Eq. (15), the boundary condition is uniquely defined if either the pyrolysis rate $\dot{m}_p$ or the total mass flow rate $\rho_w v_w$ is given. Equation (14) must be satisfied under gas–surface equilibrium as well as under nonequilibrium. However, in general, the equilibrium relationship among species concentrations conflicts with Eq. (14).

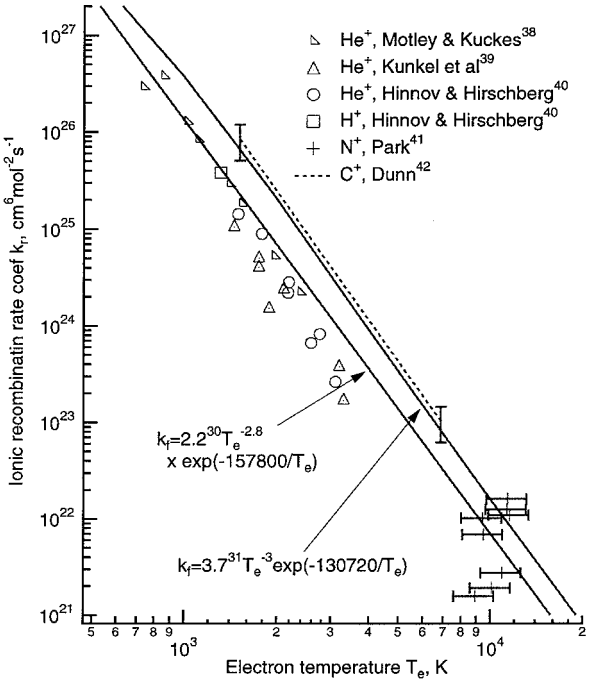


**Fig. 5 Comparison between the measured ionic recombination rates[38–42] and the expressions adopted in the present work.**

**Surface Reaction Rates**

The mass rate of change of species $i$ due to surface chemical reactions, $\dot{m}_{w,i}$, is a sum of all of those reactions involving the species. For each surface reaction, there are in general forward and reverse rates. The rate of a reverse reaction must be such that the net rate becomes zero under equilibrium for that particular reaction, according to the principle of detailed balance. If the product formed by the forward reaction is very stable, then the reverse rate calculated using the equilibrium constant becomes negligibly small.

The general method of calculating surface reaction rates is well known. The number flux of species $i$ arriving at the surface per unit surface area per unit time is given by kinetic theory as

$$I_i = n_i \sqrt{8kT_w/\pi m_i}/4$$

where $m_i$ is the mass of one species $i$ particle. If there is a surface reaction, the number of species $i$ changed by the reaction per unit surface area per unit time is obtained by multiplying $I_i$ by the probability of the reaction $\alpha_f$. The reaction probability of the reverse reaction $\alpha_r$, is related to that of the forward reaction $\alpha_f$ through the gas-phase equilibrium constant. The product

$$k_{wi} = \alpha_i \sqrt{8kT_w/\pi m_i}/4 \tag{16}$$

is called surface reaction velocity.

When an oxygen atom strikes the carbon surface, experimental evidence shows that the only significant chemical reaction to occur is the surface oxidation[47]:

$$\mathrm{O} + \mathrm{C}(s) \rightarrow \mathrm{CO} + 3.74\ \mathrm{eV}$$

Note that no $CO_2$ was found in such an experiment. The probability of this process is expressible as $0.63\exp(-1160/T_w)$ (Ref. 48). The equilibrium constant for this reaction is such that the reverse reactions need not be considered.

A parallel reaction of nitrogen-atom–carbon-surface reaction

$$\mathrm{N} + \mathrm{C}(s) \rightarrow \mathrm{CN} + 0.34\ \mathrm{eV}$$

is possible, but is hitherto unconfirmed. The equilibrium constant for this reaction is also such that the reverse reaction need not be

considered. The recombination process $N + N \rightarrow N_2$ is likely negligible because $O + O \rightarrow O_2$ is negligible.

Carbon surface sublimes at high temperatures. It is known that the sublimation product of graphite consists mostly of $C_3$ (Ref. 49). The equilibrium composition of the $C_3$ (Ref. 50) can be expressed in the temperature range of interest as

$$\gamma_{E,C3} = 1.90 \times 10^9 \exp(-59410/T_w)/(\rho_w T_w) \text{ mol/kg}$$

The coefficient $\alpha$ for the process is deduced from an experiment[49] as $\alpha = 30\exp(-21490/T_w)$. The reverse process of condensation must be included for this process.

All ions neutralize at the surface to satisfy the condition that no electrical current flows across the wall. This means that the reaction probability of neutralization is unity for all ions. Reverse reactions need not be considered also for these reactions because the equilibrium constant is very small.

By combining these, one can define the following nine surface-reaction probabilities:

$$O + C(s) \rightarrow CO: \quad \alpha_1 = 0.63\exp(-1160/T_w), \qquad m = m_O \tag{17a}$$

$$N + C(s) \rightarrow CN: \quad \alpha_2 = 0 - 1, \qquad m = m_N \tag{17b}$$

$$C(s) \rightarrow C_3: \quad \alpha_3 = 30\exp(-21490/T_w), \qquad m = m_{C3} \tag{17c}$$

$$O^+ + e \rightarrow O: \quad \alpha_4 = 1, \qquad m = m_O \tag{17d}$$

$$N^+ + e \rightarrow N: \quad \alpha_5 = 1, \qquad m = m_N \tag{17e}$$

$$C^+ + e \rightarrow C: \quad \alpha_6 = 1, \qquad m = m_C \tag{17f}$$

$$H^+ + e \rightarrow H: \quad \alpha_7 = 1, \qquad m = m_H \tag{17g}$$

$$NO^+ + e \rightarrow NO: \quad \alpha_8 = 1, \qquad m = m_{NO} \tag{17h}$$

$$N_2^+ + e \rightarrow N_2: \quad \alpha_9 = 1, \qquad m = m_{N2} \tag{17i}$$

The $\dot{m}_{w,i}$ in Eq. (14) can now be expressed in kilograms per square meter second as

$$C: \quad \dot{m}_{w,C} = k_{w6}\rho_w M_C \gamma_{C+} \tag{18a}$$

$$H: \quad \dot{m}_{w,H} = k_{w7}\rho_w M_H \gamma_{H+} \tag{18b}$$

$$O: \quad \dot{m}_{w,O} = -k_{w1}\rho_w M_O \gamma_O + k_{w4}\rho_w M_O \gamma_{O+} \tag{18c}$$

$$N: \quad \dot{m}_{w,N} = -k_{w2}\rho_w M_N \gamma_N + k_{w5}\rho_w M_N \gamma_{N+} \tag{18d}$$

$$C_3: \quad \dot{m}_{w,C3} = k_{w3}\rho_w M_{C3}(\gamma_{E,C3} - \gamma_{C3}) \tag{18e}$$

$$NO: \quad \dot{m}_{w,NO} = k_{w8}\rho_w M_{NO}\gamma_{NO+} \tag{18f}$$

$$N_2: \quad \dot{m}_{w,N2} = k_{w9}\rho_w M_{N2}\gamma_{N_2+} \tag{18g}$$

$$C^+: \quad \dot{m}_{w,C+} = -k_{w6}\rho_w M_C \gamma_{C+} \tag{18h}$$

$$H^+: \quad \dot{m}_{w,H+} = -k_{w7}\rho_w M_H \gamma_{H+} \tag{18i}$$

$$O^+: \quad \dot{m}_{w,C+} = -k_{w4}\rho_w M_C \gamma_{C+} \tag{18j}$$

$$N^+: \quad \dot{m}_{w,H+} = -k_{w5}\rho_w M_H \gamma_{H+} \tag{18k}$$

$$NO^+: \quad \dot{m}_{w,NO+} = -k_{w8}\rho_w M_{NO}\gamma_{NO+} \tag{18l}$$

$$N_2^+: \quad \dot{m}_{w,N_2^+} = -k_{w9}\rho_w M_{N2}\gamma_{N_2+} \tag{18m}$$

where the species concentration at wall $\gamma_i$ is in mole per kilogram and the density at wall $\rho_w$ is in kilogram per cubic meter. For all other species, $\dot{m}_{w,i}$ is zero.

In Eqs. (18a–18m), the reverse reactions are not included for the reasons given earlier, except for Eq. (18e). If the reverse reactions are included for all reactions, and if the $k_w$ for the reverse rates are correctly chosen to satisfy the detailed balance relationship, an equilibrium boundary condition can be obtained by arbitrarily making the reaction velocities $k_w$ very large. This equilibrium boundary condition will satisfy Eq. (14) and, therefore, is the preferred way of implementing the equilibrium boundary condition.

In Refs. 45 and 46, surface-catalytic recombination of atomic species is included in the calculation. Mass conservation dictates that the sum of probabilities for all surface reactions one species undergoes, and the probability of elastic reflection, is unity:

$$\sum_j \alpha_j + \alpha_{\text{elastic}} = 1 \tag{19}$$

For instance, oxygen atoms striking the carbon surface may react with carbon and produce CO, with a probability $\alpha_1$, or may recombine to form $O_2$, with a probability $\alpha_x$. The sum $\alpha_1 + \alpha_x$ must not be greater than unity.

The assumption of a fully catalytic wall employed in Refs. 45 and 46 is equivalent to $\alpha_x = \infty$. This violates Eq. (19). According to Eq. (19), the largest value of $\alpha$ is unity. With $\alpha = 1$, one can deduce the condition under which a surface chemical reaction for species $i$ is in equilibrium. The criterion is, from Eq. (14),

$$|\dot{m}_{w,i}| \gg \frac{\rho \bar{D}\mu_2}{\bar{M}\mu_1}\left|\frac{\partial Z_i}{\partial y}\right| \tag{20}$$

where $\dot{m}_{w,i}$ is the dominant one-way (forward or backward) rate of surface reaction for species $i$. By the using of Eqs. (18a–18m) and by the representing of the boundary-layer thickness in terms of nose radius $R$ and the Reynolds number $\rho_\infty v_\infty R/\mu_\infty$, the inequality (20) can be shown to be equivalent, to an order of magnitude, to

$$k_{wi}/v_\infty \gg \sqrt{\mu_\infty/\rho_\infty v_\infty R} \tag{21}$$

With $\alpha = 1$, the left-hand side of Eq. (21) is typically about 0.01. Therefore, for a surface reaction to be in equilibrium, the flight Reynolds number must be much larger than $1 \times 10^4$.

When condition (20) or (21) is satisfied, the rate of removal of the species involved is limited by the rate of diffusion, that is, the right-hand side of Eq. (20), rather than the rate of surface reaction. This condition is called a diffusion-limiting environment. Thus, the condition for diffusion limiting is the same as for gas–surface equilibrium.

## Sample Flowfield Calculation

**Solution by Olynick et al.[51]**

The flowfield over an ablating heat shield had been solved using a CFD method by, among others, Olynick et al.[51] The calculation accounted for $CO_2$, CO, $N_2$, $O_2$, NO, $C_2$, $C_3$, CN, $H_2$, HCN, C, N, O, H, $C^+$, $N^+$, $O^+$, and $e^-$. The reaction rate values therein are different from those in the present work. The bifurcation model was used, with the $F_i$ values given in Ref. 28. The surface values of species concentration were determined via the gas–surface equilibrium assumption and the assumption of quasi-steady-state ablation. The calculation was made for the Earth entry of the Stardust vehicle at its peak-heating point (54 s). The relative velocity and the stagnation-point pressure for this case were 11.15 km/s and 0.286 atm, respectively. The nose radius was 0.23 m. In Fig. 6, the translational and vibrational-electronic temperatures obtained are shown along the stagnation streamline.

In Fig. 7, the species molar fractions calculated are shown. The convective heating rate $q$ and the total ablation rate $\dot{m}$ were calculated to be 6.45 MW/m$^2$ and 0.089 kg/(m$^2 \cdot$ s), respectively. Of the 0.089 kg/(m$^2 \cdot$ s), surface removal rate was 0.0852 kg/(m$^2 \cdot$ s), with the remainder, 0.0038 kg/(m$^2 \cdot$ s), attributed to pyrolysis gas injection. At the wall, the elemental mass ratio was C:H:N:O = 0.4341:0.00543:0.4238:0.1419. The pyrolysis gas injection rate and the elemental fraction of hydrogen are both small because of the quasi-steady-state ablation assumption. As seen in Fig. 7, the stable species CO, $C_3$, and $N_2$ are dominant at the wall. The formation of these stable species represents a release of large amount of heat. The large concentrations of these stable species at

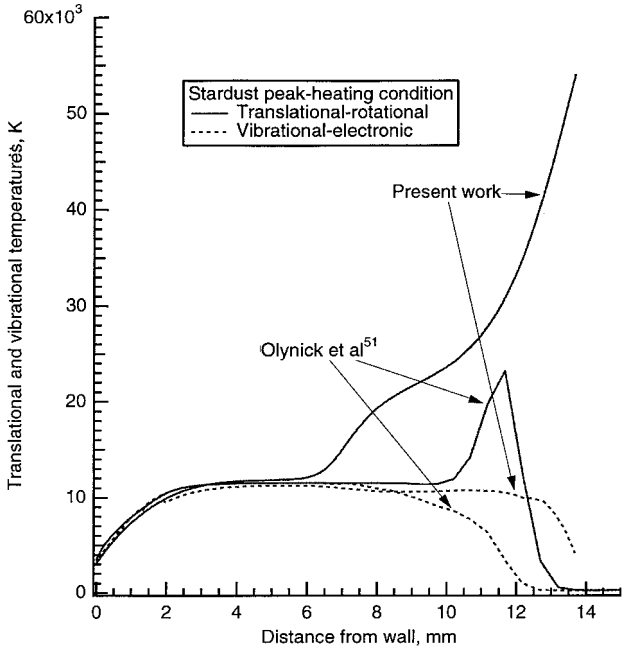


**Fig. 6 Distribution of temperatures along the stagnation streamline for the Stardust Earth entry vehicle at its peak-heating point in the trajectory obtained by Olynick et al.[51] and by present method.**

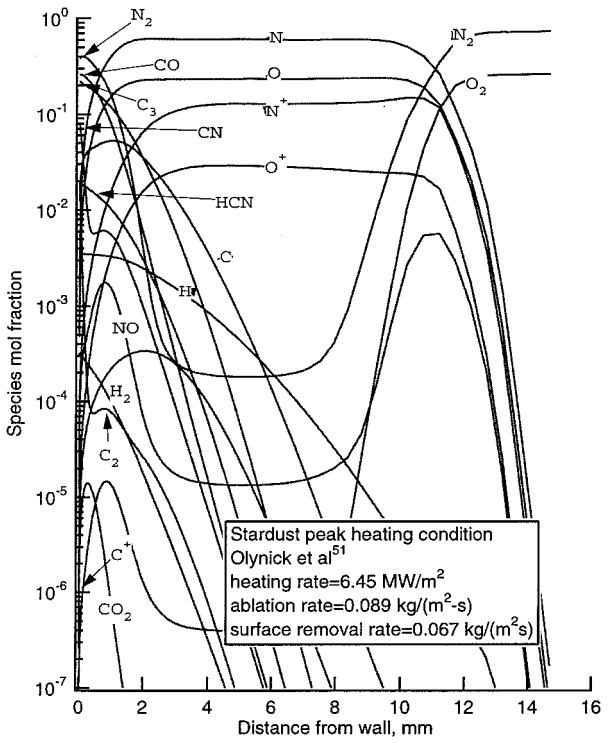


**Fig. 7 Distribution of gas species along the stagnation streamline for the Stardust Earth entry vehicle at its peak-heating point in the trajectory obtained by Olynick et al.[51]**

the wall are in turn a result of the assumptions of gas–surface equilibrium, quasi-steady-stateablation, and the choice of transport and reaction rate parameters made.

### Multicomponent Diffusion Model

To test the kinetic model developed here, sample calculations were performed for the flow along the stagnation streamline in the present work using a viscous shock layer (VSL) method[52] for the condition calculated by Olynick et al.[51] The VSL calculation accounts for two temperature thermal nonequilibrium phenomenon as described in Ref. 32. The probability of surface reaction, $\alpha_2$, producing CN, which is unknown, is varied between 0 and 1. Both the multicomponent diffusion and the bifurcation models were tested.

In the calculation with the multicomponent diffusion model, Eq. (4), an upwind differencing was used to improve stability. Nevertheless, the calculation did not produce a satisfactory result. In the beginning of the calculation, the time integration was stable. However, at a certain point, suddenly the solution became unstable. Once it became unstable, the solution diverged, and never returned to the stable mode. By the arbitrary addition of fourth-order damping term to the right-hand side of the species conservation equation, the solution became stable. However, the resulting solution was found to be unrealistic.

### Bifurcation Model

The bifurcation model [Eq. (5)] was tested with all four sets of $F_i$ values. Two sets of the chemical reaction rate coefficient $C$ for reactions 19–22, the values in Table 5 and $\frac{1}{100}$ of those, were also tested.

In Fig. 6, the temperatures calculated by the present method are compared with those calculated by Olynick et al.[51] The solution shown is for $F_i = F_{i3}$ and $\alpha_2 = 0$. There are two major differences between the two solutions. First, the translational temperature behind the shock wave in the present solution is much higher than that of Olynick et al.[51] This difference is due to the difference in calculating temperatures. In VSL, the Rankine–Hugoniot equation is solved assuming an infinitely thin shock wave; in CFD, the energy equation is solved through the shock wave (the same feature is seen, for example, in Ref. 45). Therefore, this difference is insignificant. The second difference is in the rate of approach of the two temperatures behind the shock wave: The present solution shows a slower approach. This difference is due to the difference in the transport properties and chemical reaction schemes and rates chosen. The small difference in shock standoff distance merely reflects that temperature is higher behind the shock in the present VSL solution and, therefore, is insignificant.

In Figs. 8a and 8b, the species molar fractions obtained by the present calculation are shown for the case of $F_i = F_{i3}$ for $\alpha_2 = 0$ and 1, respectively. The calculated wall heating rates are 2.494 and 3.006 MW/m$^2$ for these two cases, which are roughly half or less of that obtained by Olynick et al.[51] The low heating rate is a consequence of the low concentrations of the stable species $N_2$, CO, and $C_3$ at wall in the present solutions. The surface removal rate is 0.01809 and 0.04745 kg/(m$^2 \cdot$ s) for $\alpha_2 = 0$ and 1, respectively, which are again about half or less of the value of Olynick et al.[51] Half or more of the total ablation rate of 0.089 kg/(m$^2 \cdot$ s) is attributable in the present solutions to pyrolysis-gas injection. The low surface removal rates are a direct result of the kinetic boundary conditions used in the present work. Indirectly, the present values are affected by the transport properties and chemical reaction rates chosen.

The surface removal rate for $\alpha_2 = 1$ is two and one-half times larger than that for $\alpha_2 = 0$. The concentration of hydrogen is much larger that in the solution by Olynick et al.[51] throughout the shock layer. At the wall, the elemental mass ratio is C:H:N:O = 0.2813:0.0281:0.4473:0.2433 for $\alpha_2 = 0$, which gives a five times higher concentration of hydrogen compared with the solution by Olynick et al.[51]

The convective heat flux and the surface removal rate calculated by the present method are summarized and compared with the values of Olynick et al.[51] in Table 7. All of the present solutions are very different from the solution by Olynick et al.[51] The solutions obtained with $F_{i1}$, which is obtained with a weight of unity for all species in evaluating the standard deviation of the bifurcation model, is substantially different from other solutions. Among the solutions of $F_{i2}$–$F_{i4}$, which are obtained with the weights of 0.1, 0.01, and 0.001 for ionic species, the results are similar. The solutions with $\alpha_2 = 1$ give heating rates that are 10–20% higher and surface removal rates two and one-half times higher than those with $\alpha_2 = 0$.

The large surface removal rate for $F_i = F_{i1}$, $\alpha_2 = 1$, was found to be due to a large rate of the surface reaction N + C(s) → CN. To understand this behavior, the concentrations of N, $N^+$, and CN are

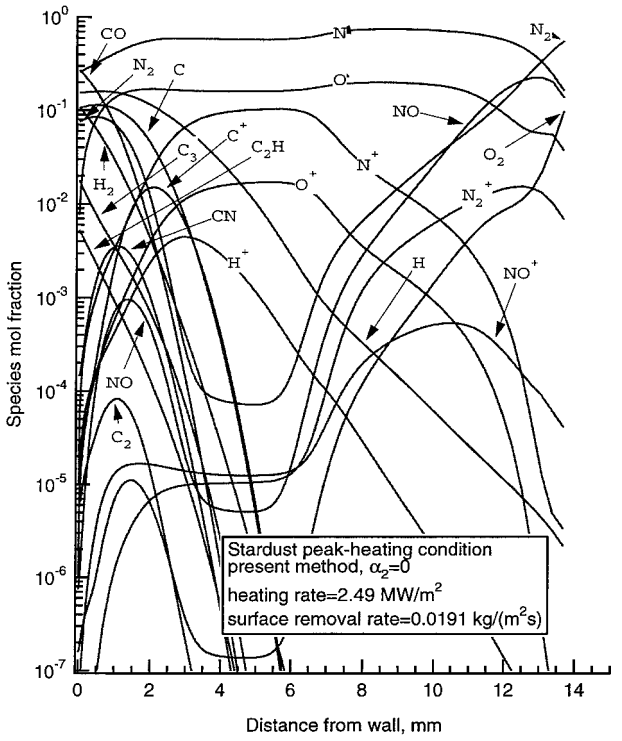


a) $\alpha_2 = 0$

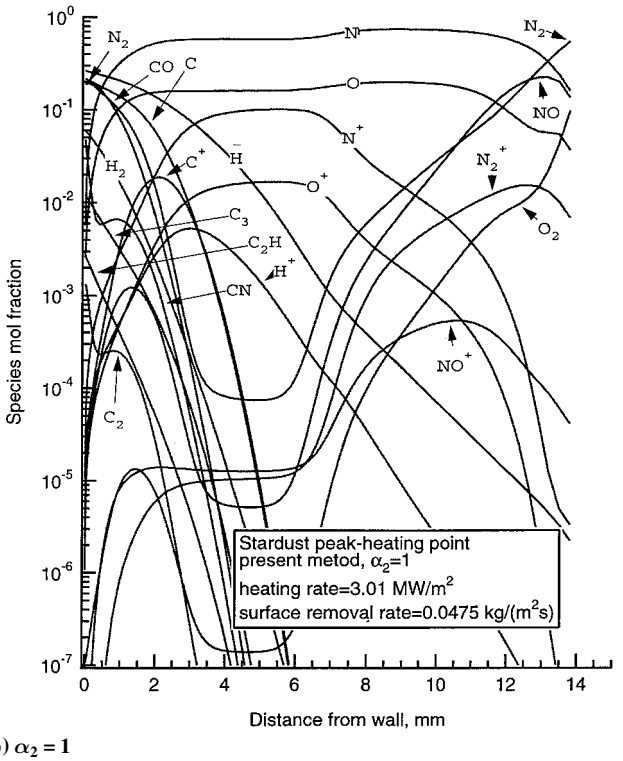


b) $\alpha_2 = 1$

**Fig. 8 Distribution of gas species along the stagnation streamline for the Stardust Earth entry vehicle at its peak-heating point in the trajectory obtained using the present model.**

compared between $F_{i3}$ and $F_{i1}$ in Fig. 9. As Fig. 9 shows, differences occur only in the concentrations of N and CN at and near the wall. Referring to Table 4, one sees that the $F_{i1}$ values for all neutral species are smaller than for other cases, leading to larger diffusion coefficients for the neutral species. Larger diffusion coefficients will cause faster supply of N and rapid removal of CN from the wall, which signifies a larger surface removal rate. On the other hand, Table 4 shows that the $F_{i1}$ values for ionic species are large, which means small diffusion coefficients. Nevertheless,

**Table 7 Comparison of stagnation region stagnation-point heating rate $q$ and surface removal rate $\dot{m}_w$ for Stardust peak heating point; $\dot{m} = 0.089$ kg/(m$^2$ ·s)**

| Rate | Olynick et al.[51] | Present calculation | | | |
|---|---|---|---|---|---|
| | | $F_{i1}$ | $F_{i2}$ | $F_{i3}$ | $F_{i4}$ |
| $q$, MW/m$^2$ | 6.45 | | | | |
| $\alpha_2 = 0$ | | 2.67 | 2.65 | 2.49 | 2.55 |
| $\alpha_2 = 1$ | | 3.33 | 2.93 | 3.01 | 2.95 |
| $\dot{m}_w$, kg/(m$^2$ · s) | 0.0862 | | | | |
| $\alpha_2 = 0$ | | 0.0288 | 0.0192 | 0.0181 | 0.0174 |
| $\alpha_2 = 1$ | | 0.0866 | 0.0421 | 0.0475 | 0.0446 |

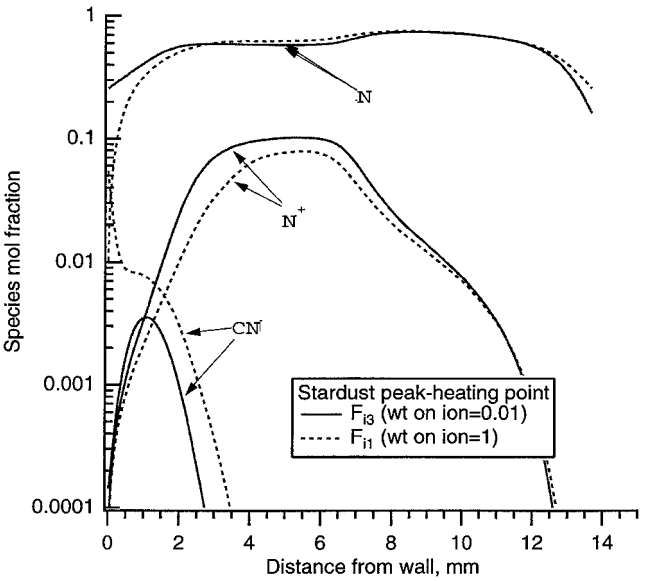


**Fig. 9 Comparison of concentrations of N, N$^+$, and CN between $F_{i3}$ and $F_{i1}$.**

Fig. 9 shows that the distribution of N$^+$ is hardly different between $F_{i1}$ and $F_{i3}$. Thus, one sees that a large error in flowfield solution is caused by a small error in $F_i$ for neutral species, but not by that for ionic species. Therefore, $F_{i2}$–$F_{i4}$, which sacrifice accuracy for the ionic species, would be a preferred choice. This also justifies the relatively inaccurate approach taken earlier in determining the collision integrals for collision pairs involving ionized species.

The calculations with the reaction rate constants with $\frac{1}{100}$ of those given in Table 5 for reactions 19–22 led to nearly identical results; they were different by less than 2% in both heating rates and surface removal rates.

## Discussion

Transport properties and gas-phase and gas–surface reaction rates are determined with the best presently possible methods. The bifurcation model parameters $F_i$ are determined with four different weights to the ionic species in the evaluation of the standard deviation of the bifurcation model from the true values. Sample calculations show that a small weight for ions is a preferred strategy in determining $F_i$. A multicomponent diffusion model is not suitable for CFD computation of flowfields.

One sees the importance of the reaction of atomic nitrogen with the carbon surface to form CN. The heating rate is increased slightly, but the surface removal rate is increased two and one-half times by this reaction. Determination of the probability of this reaction is desirable.

Finally, note that, even though the heating and surface removal rates predicted by the present work are smaller than those values predicted earlier, such as by Olynick et al.,[51] the true total heating and surface removal rates in flight may not be lower. In such past calculations, radiative heating rates were calculated assuming that

radiation emanates from the air species. References 5 and 53 suggest that radiation may emanate mostly from carbonaceous species in an ablating environment, and its intensity may be much higher. Until this aspect of the problem is understood, one should withold judgement on the appropriateness of the current method of designing ablative heat shields.

## Conclusions

The transport property value set, the chemical reaction rate coefficient set, and the parameter set for the bifurcation model and for the kinetic wall boundary conditions are derived for the ablating environment using the best available methods. The present set of parameters leads to heating and surface removal rates that are one-half or less of the values obtained earlier by the use of the assumptions of gas–surface equilibrium and quasi-steady-state ablation. In applying the bifurcation model, the $F_i$ parameter obtained with a small weight to the ionic species is recommended. The multicomponent diffusion model leads to instability in the time integration of the conversation equations. Formation of CN by the reaction of atomic nitrogen with solid carbon could increase the surface removal rate by a factor of two and one-half.

## Acknowledgment

The first author wishes to acknowledge the support provided by NASA Ames Research Center through Contract NAS2-99092 to Eloret Corporation.

## References

[1]Olynick, D. R., "Aerothermodynamics of the Stardust Sample Return Capsule," AIAA Paper 98-0167, Jan. 1998.

[2]Gupta, R. N., "Aerothermodynamic Analysis of Stardust Sample Return Capsule with Coupled Radiation and Ablation," AIAA Paper 99-0227, Jan. 1999.

[3]Park, C., Abe, T., and Inatani, Y., "Research on the Heatshield for MUSES-C Earth Reentry," AIAA Paper 98-2852, June 1998.

[4]Desnoyer, D., Buck, C., and Larrieu, J. M., "CNSR Rosetta SEPCORE—A Breakthrough for Earth Reentry Capsule," International Astronautical Federation, IAF Paper 91-298, Oct. 1991.

[5]Park, C., and Tauber, M. E., "Heatshielding Problems of Planetary Entry, A Review," AIAA Paper 99-3415, June 1999.

[6]Balakrishnan, A., Park, C., and Green, M. J., "Radiative Viscous-Shock-Layer Analysis of Fire, Apollo, and PAET Flight Data," *Thermophysical Aspects of Re-Entry Flows*, edited by J. N. Moss and C. D. Scott, Vol. 103, Progress in Astronautics and Aeronautics, AIAA, New York, 1986, pp. 514–570.

[7]Gupta, R. N., Lee, K.-P., Moss, J. N., and Sutton, K., "Viscous Shock-Layer Solutions with Coupled Radiation and Ablation for Earth Entry," *Journal of Spacecraft and Rockets*, Vol. 29, No. 2, 1992, pp. 173–181.

[8]Curry, D. M., and Stephens, E. W., "Apollo Ablator Thermal Performance at Superorbital Entry Velocities," NASA TN D-5969, Sept. 1970.

[9]Ahn, H. K., Park, C., and Sawada, K., "Dynamics of Pyrolysis Gas in Charring Materials Ablation," AIAA Paper 98-0165, Jan. 1998.

[10]"User's Manual: Aerotherm Chemical Equilibrium Computer Program," Acurex Corp., Mountain View, CA, Aug. 1981.

[11]Kendall, R. M., Bartlett, E. P., Rindal, R. A., and Moyer, C. B., "An Analysis of the Coupled Chemically Reacting Boundary Layer and Charring Ablator, Part 1. Summary Report," NASA CR-1060, June 1969.

[12]Cooper, D. M., and Jones, J. J., "An Experimental Determination of the Cross Section of the Swing Band System of C3," *Journal of Quantitative Spectroscopy and Radiative Transfer*, Vol. 22, No. 8, 1979, pp. 201–208.

[13]Shinn, J. L., "Optical Absoprtion of Carbon and Hydrogen Species from Shock Heated Acetylene and Methane in the 135-220 nm Wavelength Range," AIAA Paper 81-1189, June 1981.

[14]Gupta, R. N., Yos, J. M., Thompson, R. A., and Lee, K., "A Review of Reaction Rates and Thermodynamic and Transport Properties for an 11-Species Air Model for Chemical and Thermal Nonequilibrium Calculations to 30,000 K," NASA Reference Publ. 1232, Aug. 1990.

[15]Levin, E., Partridge, H., and Stallcop, J. R., "Collision Integrals and High Temperature Transport Properties for N–N, O–O, and N–O," *Journal of Thermophysics and Heat Transfer*, Vol. 4, No. 4, 1990, pp. 469–477.

[16]Stallcop, J. R., Bauschlicher, C. W., Jr., and Partridge, H., "Theoretical Study of Hydrogen and Nitrogen Interactions: N–H Transport Cross Sections and Collision Integrals," *Journal of Chemical Physics*, Vol. 97, No. 8, 1992, pp. 5578–5585.

[17]Stallcop, J. R., and Partridge, H., "Resonance Charge Transfer, Transport Cross Sections, and Collision Integrals for $N^+(^3P)$–$N(^4S^0)$ and $O^+(^4S^0)$–$O(^3P)$ Interactions," *Journal of Chemical Physics*, Vol. 95, No. 9, 1991, pp. 6429–6439.

[18]Partridge, H., and Stallcop, J. R., "Transport Cross Sections and Collision Integrals for $N(^4S^0)$–$O^+(^4S^0)$ and $N^+(^3P)$–$O(^3O)$ Interactions," *Chemical Physics Letters*, Vol. 184, No. 5, 6, 1991, pp. 505–512.

[19]Stallcop, J. R., Partridge, H., Walch, S. P., and Levin, E., "H–$N_2$ Interaction Inergies, Transport Cross Sections, and Collision Integrals," *Journal of Chemical Physics*, Vol. 97, No. 5, 1992, pp. 3431–3436.

[20]Stallcop, J. R., Partridge, H., and Levin, E., "H–$H_2$ Collision Integrals and Transport Coefficients," *Chemical Physics Letters*, Vol. 254, No. 1, 2, May 1996, pp. 25–31.

[21]Stallcop, J. R., Partridge, H., Pradhan, A., and Levin, E., "Potential Energies, Transport Cross Sections, and Collision Integrals for Interaction of Carbon and Nitrogen Atoms," *Journal of Thermophysics and Heat Transfer*, Vol. 14, No. 4, 2000, pp. 480–488.

[22]Williams, J. F., "Electron Scattering from Hydrogen Atoms 2. Elastic Scattering at Low Energies from 0.5 to 8.7 eV," *Journal of Physics B*, Vol. 8, No. 10, 1975, pp. 1683–1687.

[23]Thomas, L. D., and Nesbet, R. K., "Low-Energy Electron Scattering by Atomic Oxygen," *Physical Review A*, Vol. 11, No. 1, 1975, pp. 170–173.

[24]Thomas, L. D., and Nesbet, R. K., "Low-Energy Electron Scattering by Atomic Nitrogen," *Physical Review A*, Vol. 12, No. 6, 1975, pp. 2369–2377.

[25]Thomas, L. D., and Nesbet, R. K., "Low-Energy Electron Scattering by Atomic Carbon," *Physical Review A*, Vol. 12, No. 6, 1975, pp. 2378–2382.

[26]Hirschfelder, J. O., Curtiss, C. F., and Bird, R. B., *Molecular Theory of Gases and Liquids*, Wiley, New York, 1954, pp. 715, 1126, 1127.

[27]Svehla, R. A., "Estimated Viscosities and Thermal Conductivities of Gases at High Temperatures," NASA TR R-132, 1962.

[28]Kendall, R. M., Bartlett, E. P., Rindal, R. A., and Moyer, C. B., "An Analysis of the Coupled Chemically Reacting Boundary Layer and Charring Ablator, Part 4. A Unified Approximation for Mixture Transport Properties for Multicomponent Boundary-Layer Applications," NASA CR-1063, 1969.

[29]Yos, J. M., "Transport Properties of Nitrogen, Hydrogen, Oxygen, and Air, to 30,000 K," AVCO Corp., RAD–TM 63-7, Wilmington, MA, March 1963.

[30]Ramshaw, J. D., and Chang, C. H., "Ambipolar Diffusion in Two-Temperature Multicomponent Plasmas," *Plasma Chemistry and Plasma Processing*, Vol. 13, No. 3, 1993, pp. 489–498.

[31]Bird, R. B., "Diffusion in Multicomponent Gas Mixtures," *Kagaku Kogaku*, Vol. 26, No. 11, 1962, pp. 718–721.

[32]Park, C., *Nonequilibrium Hypersonic Aerothermodynamics*, Wiley, New York, 1990, p. 326.

[33]Park, C., Howe, J. T., Jaffe, R. L., and Candler, G. V., "Chemical-Kinetic Problems of Future NASA Missions. II. Mars Entries: A Review," *Journal of Thermophysics and Heat Transfer*, Vol. 8, No. 1, 1994, pp. 9–23.

[34]Baulch, D. L., Drysdale, D. D., and Horne, D. G., *Evaluated Kinetic Data for High Temperature Reactions, Vol. 1, Homogeneous Gas Phase Reactions of the $H_2$-$O_2$ System*, CRC Press, Boca Raton, FL, 1972.

[35]Oldenborg, R., Chinitz, W., Friedman, M., Jachimowski, C., Rabinowitz, M., and Schott, G., "Status Report of the Rate Constant Committee, NASP High Speed Propulsion Technology Team," Dec. 1989.

[36]Bose, D., and Candler, G. V., "Thermal Rate Constants of the $N_2 + O \rightarrow NO + N$ Reaction Using *ab initio* $^3A''$ and $^3A'$ Potential Energy Surfaces," *Journal of Chemical Physics*, Vol. 104, No. 8, 1996, pp. 2825–2833.

[37]Bose, D., and Candler, G. V., "Thermal Rate Constants of the $O_2 + N \rightarrow NO + O$ Reaction Using *ab initio* $^2A''$ and $^4A'$ Potential Energy Surfaces, *Journal of Chemical Physics*, Vol. 107, No. 16, 1997, pp. 6136–6145.

[38]Kuckes, A. F., and Motley, R. W., "Recombination in a Helium Plasma," NASA Rept. MATT-71, May 1961.

[39]Kunkel, W. B., Robben, F., and Talbot, L., "Spectroscopic Study of Electron Recombination with Monatomic Ions in a Helium Plasma," *Physical Review 2nd Series*, Vol. 132, No. 12, 1963, pp. 2363–2371.

[40]Hinnov, E., and Hirschberg, J. G., "Electron-Ion Recombination in Dense Plasmas," *Physical Review*, Vol. 125, No. 3, 1961, pp. 795–801.

[41]Park, C., "Measurement of Ionic Recombination of Nitrogen," *AIAA Journal*, Vol. 6, No. 11, 1968, pp. 2090–2094.

[42]Dunn, M. G., "Measurement of $C^+ + e + e$ and $CO^+ + e$ Recombination in Carbon Dioxide Flows," *AIAA Journal*, Vol. 9, No. 11, 1971, pp. 2184–2191.

[43]Kondratiev, V. N., *Rate Constants of Gas Phase Reactions*, Office of Standard Reference Data, National Bureau of Standards, Washington, DC, Jan. 1972.

[44]Kendall, R. M., Bartlett, E. P., Rindal, R. A., and Moyer, C. B., "An Analysis of the Coupled Chemically Reacting Boundary Layer and Charring Ablator, Part 1. Summary Report," NASA CR-1060, 1969.

[45]Gupta, R. N., "Viscous Shock-Layer Study of Thermochemical Nonequilibrium," *Journal of Thermophysics and Heat Transfer*, Vol. 10, No. 2, 1996, pp. 257–266.

[46]Chen, Y. K., and Milos, F. S., "Ablation and Thermal Response Program for Spacecraft Heat Shield Analysis," AIAA Paper 98-0273, Jan. 1998.

[47]Liu, G., "High Temperature Oxidation of Graphite by a Dissociated Oxygen Beam," Ph.D. Thesis, Dept. of Aeronautics and Astronautics, Massachusetts Inst. of Technology, Cambridge, MA, Sept. 1973.

[48]Park, C., *Nonequilibrium Hypersonic Aerothermodynamics*, Wiley, New York, 1990, p. 349.

[49]Baker, R. L., McDonaugh, J. M., Herr, K. C., Klingberg, R. A., Coffer, J. C., and Covington, M. A., "Carbon Vaporization Condensation Effects," NASA TM 874300, July 1984.

[50]Chase, M. W., Davies, C. A., Downey, J. R., Jr., Frurip, D. J., McDonald, R. A., and Syverud, A. N., "JANAF Thermochemical Tables, Third Edition, Parts 1 and 2," *Journal of Physical and Chemical Reference Data*, Vol. 14, Supplement 1, 1985.

[51]Olynick, D. R., Chen, Y. K., and Tauber, M. E., "Forebody TPS Sizing with Radiation and Ablation for the Stardust Sample Return Capsule," AIAA Paper 97-2474, June 1997.

[52]Park, C., and Ahn, H. K., "Stagnation-Point Heat Transfer Rates for Pioneer-Venus Probes," *Journal of Thermophysics and Heat Transfer*, Vol. 13, No. 1, 1999, pp. 33–41.

[53]Park, C., "Interaction of Spalled Particles with Shock Layer Flow," *Journal of Thermophysics and Heat Transfer*, Vol. 13, No. 4, 1999, pp. 441–449.